HHS Public Access

Author manuscript

Cell. Author manuscript; available in PMC 2022 February 18.

Published in final edited form as:

Cell. 2021 February 18; 184(4): 969–982.e13. doi:10.1016/j.cell.2021.01.024.

A role of PIEZO1 in iron metabolism in mice and humans

Shang Ma[1], **Adrienne E Dubin**[1], **Yunxiao Zhang**[1], **Seyed Ali Reza Mousavi**[1], **Yu Wang**[1], **Adam Coombs**[1], **Meaghan Loud**[1], **Immacolata Andolfo**[2], **Ardem Patapoutian**[1,3]

[1]Howard Hughes Medical Institute, Department of Neuroscience, Dorris Neuroscience Center, Scripps Research, La Jolla, CA 92037, USA.

[2]Department of Molecular Medicine and Medical Biotechnologies, Federico II" University of Naples, CEINGE - Biotecnologie Avanzate, Naples, Italy.

[3]Lead contact

Summary

Iron overload causes progressive organ damage and is associated with diseases including arthritis, liver and heart failure. Elevated iron levels are present in 1–5% of individuals; however, iron overload is undermonitored and underdiagnosed. Genetic factors affecting iron homeostasis are emerging. Individuals with hereditary xerocytosis, a rare disorder with gain-of-function (GOF) mutations in mechanosensitive PIEZO1 ion channel, develop age-onset iron overload. We show that constitutive or macrophage expression of a GOF *Piezo1* allele in mice disrupts levels of the iron regulator hepcidin and causes iron overload. We further show that PIEZO1 is a key regulator of macrophage phagocytic activity and subsequent erythrocyte turnover. Strikingly, we find that E756del, a mild GOF *PIEZO1* allele present in a third of individuals of African descent, is strongly associated with increased plasma iron. Our study links macrophage mechanotransduction to iron metabolism and identifies a genetic risk factor for increased iron level in African Americans.

Graphical Abstract

*Correspondence to: Ardem Patapoutian (ardem@scripps.edu).

Author contributions:

A.P. and S.M. designed experiments and wrote the paper. S.M. performed all mouse experiments and human blood measurements. A.E.D. performed electrophysiology experiments. Y.X.Z. ,Y.W. and S.M. performed and analyzed cytometry experiments. S.A.R. and S.M. did immunocytochemistry staining and analysis. A.C. performed *in situ* hybridization. S.A.R. and S.M. genotyped human samples. M.L. and A.C. performed mouse genotyping. I.A. contributed by discussing experimental details.

Declaration of Interests

The authors declare no competing interests.

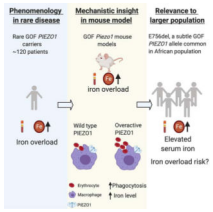

Introduction

Iron is essential for cellular processes such as hemoglobin biosynthesis for oxygen transport. However, too much iron is toxic to organs (Dabbagh et al., 1993; Gujja et al., 2010; Milic et al., 2016), thus iron levels are tightly controlled by homeostatic processes (Fleming and Ponka, 2012; Ganz, 2013). Iron homeostasis involves the action of multiple cell types, and key players include enterocytes, red blood cells (RBCs), macrophages and hepatocytes. Many pathways involved in iron metabolism are emerging (Andrews and Ganz, 2019). However, the genetic factors that predispose people to iron overload are not well understood.

The majority of circulating iron is derived from recycling of RBCs, which contain hemoglobin, the primary iron reservoir. Macrophages in the spleen and liver clear senescent RBCs via phagocytosis and release iron from heme after chemical breakdown of hemoglobin (Ganz, 2012). This highly dynamic process recycles ~25 mg of iron per day, and accounts for the vast majority of total serum iron in the blood (Korolnek et al., 2015; Fleming and Ponka, 2012). By contrast, enterocytes of the small intestine absorb 1–2 mg of dietary iron per day, so iron absorption in the digestive tract accounts for only 5–10% of total iron in the bloodstream (Fleming and Ponka, 2012).

Many of the key players in regulating iron homeostasis have been identified. Transferrin is a blood plasma protein that binds and transports circulating iron into tissues via transferrin receptor-mediated endocytosis (Gomme et al., 2005). Once internalized into cells, iron is bound by ferritin, a protein that sequesters iron. Since ferritin is also secreted extracellularly, serum ferritin levels are also used as a clinical marker for total body iron store (Knovich et al., 2009). Hepatocytes in the liver are the major iron storage sites and important sensors of iron levels. In response to elevated iron in the liver, hepatocytes transcribe a gene encoding the peptide hormone hepcidin, the master regulator of iron metabolism (Park et al., 2001; Ganz, 2011). Hepcidin suppresses the release of iron from enterocytes and macrophages into the blood via down-regulating iron transporter ferroportin activity (Donovan et al., 2005; Ganz and Nemeth, 2012a). In principle, iron overload can result from disruption of any step of these multicellular processes. People suspected of iron overload receive laboratory blood tests for transferrin and ferritin, but accurate clinical diagnosis of iron overload requires an expensive magnetic resonance imaging (MRI) scan (Fleming and Ponka, 2012). Furthermore, the treatment for iron overload is limited to two elementary therapeutic options– phlebotomy and iron chelation, and their effectiveness is limited by high costs and a wide range of side effects (Mobarra et al., 2016). Thus, iron overload is underdiagnosed and has a dearth of treatment options.

Iron overload can have genetic or iatrogenic (e.g. from blood transfusions) origins. Hereditary hemochromatosis is the most common inherited form of iron overload with around 1 million people affected in the United States (Brissot et al., 2018). It is most frequently caused by mutations in *HFE* gene, encoding the human hereditary hemochromatosis protein (HFE) (Feder et al., 1996). HFE interacts with transferrin receptors to regulate transferrin-bound iron uptake and hepcidin expression (Roy et al., 1999). The *HFE* C282Y allele is the most prevalent mutation associated with iron overload: 10% of individuals of northern European descent are C282Y heterozygotes and 0.3 – 0.5% are homozygotes. A large-scale study found that C282Y homozygosity, but not heterozygosity, is associated with elevated transferrin saturation and ferritin, indicating higher risks for iron overload (Adams et al., 2005). A recent study found that C282Y carriers have higher risks for multi-organ complications such as diabetes, obesity and arthritis (Pilling et al., 2019). However, the C282Y allele cannot account for high serum iron in people of non-European ancestry. For example, studies have suggested that around 5% or 10% of individuals of African descent have high transferrin saturation levels and high serum ferritin respectively, but the frequency of C282Y homozygosity in African populations is extremely low at 0.01% (Adams et al., 2005). Therefore, unknown genetic factors play important but unrecognized roles in iron overload in African population.

Mechanisms beyond HFE and transferrin pathway could contribute to iron metabolism deficiencies in humans. For example, iron overload is sometimes a complication of other blood disorders. Indeed, hemoglobin deficits in β-thalassemia patients cause iron overload secondary to RBC defects, irrespective of whether these individuals receive blood transfusions (Hershko, 2010; Taher and Saliba et al., 2017). Recently, iron overload was also observed in patients with hereditary xerocytosis (HX), another blood disorder that causes red blood cell (RBC) dehydration with mild hemolysis (Andolfo et al., 2020; Picard et al., 2019). Intriguingly, HX is associated with gain-of-function (GOF) mutations in PIEZO1, a mechanically activated non-selective cation channel (Coste et al., 2010; Albuisson et al., 2013; Zarychanski et al., 2012). PIEZO1 and PIEZO2 are crucial mechanotransducers in vertebrates. PIEZO2 is the principal mechanosensitive channel responsible for touch, proprioception, and baroreception (Ranade et al., 2014; Woo et al., 2015; Zeng et al., 2018), while PIEZO1 plays an essential role in cardiovascular development, RBC cell volume, and bone formation (Ranade et al., 2014; Li et al., 2014; Cahalan et al., 2015; Sun et al., 2019).

The association between HX and iron overload, combined with our recent discovery of GOF mutations in *PIEZO1* in HX, presented the opportunity to investigate whether PIEZO1 directly participates in iron homeostasis, aside from its known roles in RBC physiology. Moreover, a common *PIEZO1* GOF mutation (E756del) previously identified by our group is observed in up to one third of individuals of west African descent from different geographic regions and is associated with a mild form of RBC dehydration (Ma et al., 2018). The prevalence of this allele in most African populations raises the possibility that iron overload observed in rare HX patients is also relevant to a much larger population, and provides us with a large pool of individuals to study the effect of GOF PIEZO1 in iron homeostasis. We therefore investigated the link between GOF PIEZO1 and iron overload in a mouse model of HX (Ma et al., 2018; Picard et al., 2019). Is iron overload merely a consequence of RBC dehydration in HX? Or does PIEZO1 in other cell types contribute to

iron homeostasis? In this work, we combine mouse and human genetics to answer these questions.

Results

Gain-of-function *Piezo1* mice develop age-onset iron overload.

Previously, we generated mice that express a Cre-dependent human-equivalent gain-of-function (GOF) *PIEZO1* allele and showed that these transgenic mice model hereditary xerocytosis (HX), a rare blood disorder primarily characterized by dehydrated red blood cells (RBCs; Ma et al., 2018). Aging HX patients develop iron overload (Andolfo et al., 2020; Picard, 2019). Here, we first tested if the constitutive GOF *Piezo1* mice also develop age-onset iron overload (Ma et al., 2018; Schwenk et al., 1995). A hallmark of iron overload is the presence of excessive iron in the liver (Fleming and Ponka, 2012). We performed a histological analysis of liver with Perls Prussian blue that detects iron (Parmley et al., 1978). Iron staining was observed in hepatocytes of constitutive heterozygous GOF *Piezo1* aging mice (over 1 year old); interestingly, even higher levels were detected in liver Kupffer cells (macrophages) (Figure 1A). As expected, no staining was observed in wild-type littermates (Figure 1A). Iron deposition was more severe in homozygous GOF *Piezo1* mice than in heterozygous mice (Figure 1A). We next used an enzymatic assay to quantify iron levels in liver extracts. As expected, we found that aging wild-type mice had minimal liver iron levels; however, aging GOF *Piezo1* mice had elevated levels (Figure 1B, right of the dashed line). Consistent with the histological analysis, homozygote livers had substantially higher liver iron levels compared to heterozygotes (Figure 1B). Interestingly, we found that heterozygous or homozygous young adult GOF *Piezo1* mice (2 – 5 months old) did not show increased liver iron content compared to wild-type controls (Figure 1B, left of the dashed line).

In addition to excessive iron storage in liver, iron overload is associated with elevated serum iron levels. We measured the serum iron concentration in both aging and young adult mice. We found that aging GOF *Piezo1* mice had significantly higher serum iron concentration than wild-type controls, with homozygotes more severely affected than heterozygotes (Figure 1C). Similar to liver iron accumulation, we found that serum iron elevation did not occur in young adult GOF *Piezo1* mice (Figure 1C).

Transferrin saturation, measured as a percentage, is the serum iron amount divided by the total iron-binding capacity of the available transferrin, reflects how much serum iron is bound by transferrin, and correlates with serum iron level (Fleming and Ponka, 2012). Similar to findings with total serum iron concentrations, we found that aging GOF *Piezo1* mice, but not young adults, had significantly higher transferrin saturation values (Figure 1D). Finally, ferritin concentration in the blood reflects the amount of iron stored in the body, and together with transferrin saturation, serves as a provisional test for iron overload (Jensen, 2004). Once again, we found that only aging GOF *Piezo1* mice had significantly increased ferritin levels (Figure 1E). Therefore, we show with combined evidence from liver iron accumulation, serum iron levels, transferrin saturation, and ferritin concentration that GOF *Piezo1* mice fully recapitulate the age-onset iron overload phenotype observed in the

rare HX patients. Therefore, our transgenic model provides a useful tool for further investigation of how PIEZO1 contributes to iron metabolism.

Gain-of-function PIEZO1 expression in macrophages causes iron overload.

We next sought to elucidate the cell type in which GOF PIEZO1 expression causes iron overload. Blood iron level is tightly controlled by interplay between red blood cells (RBCs), macrophages, and hepatocytes (Fleming and Ponka, 2012; Muckenthaler et al, 2017). PIEZO1 is not highly expressed in hepatocytes in mice (Figure S1A), but is robustly expressed in RBCs (Cahalan et al., 2015) and macrophages (Solis et al., 2019) (Figure S1B); we therefore tested the requirement of GOF PIEZO1 in these two cell types. Since RBCs are the major reservoirs for iron in the form of hemoglobin and iron overload often accompanies RBC disorders (Taher and Saliba et al., 2017), we initially suspected that the iron overload phenotype observed in GOF *Piezo1* mice is secondary to RBC dehydration. To test this, we analyzed mice expressing GOF PIEZO1 only in red blood cells (Ma et al., 2018; Heinrich et al., 2004). Surprisingly, we found that aging heterozygous RBC-specific GOF *Piezo1* mice did not accumulate noticeable iron deposits in the liver (Figure 2A, left panels). In addition, aging heterozygous and homozygous RBC-specific GOF *Piezo1* mice had liver iron levels similar to wild type controls (Figure 2B, left of the dashed line). Consistently, serum iron levels, transferrin saturation, and ferritin concentrations were all normal in aging RBC-specific GOF *Piezo1* mice (Figure 2C–E, left of the dashed lines). The evidence from liver and serum iron suggests that RBC dehydration is unlikely to be the main cause for late-onset iron overload in HX animal model.

Macrophages are phagocytic cells that play diverse homeostatic roles in addition to their well-known contributions to the innate immune system. Specialized tissue-resident macrophages of the liver and spleen phagocytose senescent RBCs and subsequently break down hemoglobin to release iron into the bloodstream (Ganz, 2012). This recycling process converts stored iron into a bioavailable form. PIEZO1-dependent mechanosensation in macrophages has been previously implicated in innate immunity in the lung (Solis et al, 2019), however its role in phagocytosis or homeostatic functions of macrophages is wholly unknown. We tested mice expressing GOF PIEZO1 in macrophages by using LysM-cre that targets myeloid cells (Clausen et al., 1999). Remarkably, we observed increased iron deposition in the livers (both hepatocytes and Kupffer cells) of aging macrophage-specific *Piezo1* GOF mice that was more pronounced in homozygotes than in heterozygotes (Figure 2A, middle and right panels). Our quantitative analysis showed that liver iron content from aging macrophage-specific GOF *Piezo1* mice was indistinguishable from constitutive GOF *Piezo1* mice, for both heterozygotes and homozygotes (Figure 1B and 2B, right of the dashed lines). In addition, serum iron levels, transferrin saturation, and ferritin concentration in aging macrophage-specific GOF *Piezo1* mice were all elevated compared to aging wild-type littermate controls (Figure 2C–E, right of the dashed lines). Importantly, these serum iron measurements in macrophage-specific *Piezo1* mice are comparable to the values observed in mice constitutively expressing GOF PIEZO1 (compare Figure 2C–E to Figure 1C–E).

We also tested if macrophages with overactive PIEZO1 indirectly cause iron disorder via RBC abnormalities. Whole blood count analysis showed that macrophage-specific GOF *Piezo1* mice had normal RBC numbers, hematocrit (HCT), and mean corpuscular hemoglobin concentration (MCHC) and volume (MCV) (Figure S2). Thus, GOF PIEZO1 in macrophages is unlikely to induce RBC damage. Together, our study of RBC- and macrophage- specific GOF *Piezo1* mice suggests that GOF PIEZO1-induced iron overload is due to its action in macrophages and not in RBCs. Although LysM-cre targets all myeloid cells, GOF PIEZO1 is likely to cause iron overload via actions in macrophages which have well-established functions in iron metabolism.

Hepcidin levels are decreased in macrophage-specific gain-of-function *Piezo1* mice.

The small peptide hormone hepcidin is a key regulator of iron metabolism in mammals (Ganz, 2011). Secreted hepcidin protein from hepatocytes suppresses the release of iron into the blood, and chronically reduced hepcidin levels induce iron overload (Papanikolaou et al., 2005). We found that hepcidin transcript levels in liver extracts were dramatically reduced in aging macrophage-specific GOF *Piezo1* mice (Figure 3A). In addition, we found that serum hepcidin protein concentration was significantly lower in aging macrophage-specific GOF *Piezo1* mice compared to wild-type littermates when measured by enzyme-linked immunosorbent assay (ELISA; Figure 3B). Interestingly, we detected a statistically significant reduction in both liver hepcidin transcript levels and serum hepcidin protein concentration in young adult macrophage-specific GOF *Piezo1* mice (Figure 3C and 3D), although this decrease was less dramatic than what was observed in aging mice. These data indicate that compromised hepcidin levels in young adult mice (which have normal iron levels) precede iron overload in aging GOF mice, and suggest that dysregulation of the hepcidin pathway is a key instigator of iron overload in the HX model.

Acute response to iron stress is compromised in macrophage-specific gain-of-function *Piezo1* mice

The temporal relationship between hepcidin reduction and the presence of iron overload also suggests that the age-onset iron overload might be due to continued dysregulation of iron metabolism throughout adulthood. To test this possibility, we challenged young adult mice with acute iron stress. We performed a single intraperitoneal injection of iron dextran at 40 μg per gram body weight in adult mice (Zhang et al., 2011). This single-dose treatment was not sufficient to alter serum iron levels, transferrin saturation, or ferritin concentration in young adult wild-type mice after 24 hours (Figure 4A–C). In contrast, all tested blood parameters were elevated in heterozygous constitutive GOF *Piezo1* mice after a single injection (Figure 4A–C). Importantly, macrophages-, but not RBC-specific GOF *Piezo1* mice fully phenocopied the increased serum iron levels, transferrin saturation, and ferritin concentration observed in constitutive GOF *Piezo1* mice in response to iron stress (Figure 4A–C). These results indicate that overactive PIEZO1 in macrophages not only causes iron overload in aging mice but also disrupts the acute response to excessive iron in young adult mice.

Next, we tested whether hepcidin levels are associated with the observed acute iron dysregulation. We found that acute iron stress significantly increased liver hepcidin

transcript levels and serum hepcidin protein concentration in adult wild-type mice, as expected (Figure 4D and Figure S3). However, there was no significant increase in hepcidin transcript or protein in macrophage-specific GOF *Piezo1* adult mice (Figure 4D and Figure S3), indicating that hepcidin induction is impaired in macrophage-specific GOF *Piezo1* mice. Therefore, the acute iron stress experiment suggests that mice with overactive PIEZO1 in macrophages develop age-onset iron overload due to chronically impaired iron regulation during adulthood.

Gain-of-function PIEZO1 in macrophages enhances erythropoiesis, red blood cell turnover and phagocytic activity.

But how does overactive PIEZO1 in macrophages affect hepcidin levels? Hepcidin coordinates iron metabolism to meet the demand for RBC production (Pasricha et al., 2016; Ganz and Nemeth, 2012b): it is down-regulated during increased erythropoiesis to ensure sufficient iron availability for new hemoglobin synthesis. We hypothesized that GOF PIEZO1 in macrophages increases erythropoiesis which inhibits hepcidin production. Indeed, despite normal mature RBC properties (Figure 2S), macrophage-specific GOF *Piezo1* mice had a significantly higher reticulocyte count (Figure 5A), an indicator of enhanced erythropoiesis. Erythroferrone, produced from bone marrow and the spleen, is a hormone that down-regulates liver hepcidin expression during enhanced erythropoiesis (Kautz et al., 2014; Kautz et al., 2015). Remarkably, we observed that serum erythroferrone levels were significantly increased in adult macrophage-specific GOF *Piezo1* mice compared to the almost undetectable levels found in wild types (Figure 5B). Thus, macrophages with overactive PIEZO1 enhance erythropoiesis and increase erythroferrone to reduce hepcidin expression. A higher reticulocyte but normal mature RBC count suggests a chronically increased RBC turnover rate (i.e. due to enhanced phagocytosis of RBCs) in macrophage-specific GOF *Piezo1* mice. To test the *in vivo* rate of RBC turnover via phagocytosis, we measured the half-life of RBCs using a pulse-chase experiment. We intravenously injected 5×10^7 fluorescently labeled RBCs into adult mice (equivalent to ~ 1–2% of the total RBC content of whole blood), collected blood samples at specific time points over several weeks, and measured the number of labeled RBCs by flow cytometry. The number of labeled RBCs declines over time as the cells age and are cleared from the circulation by phagocytosing macrophages (Dholakia et al., 2015) (Figure S4A). The number of fluorescent RBCs declined over a three-week period in adult wild type mice to about 50% of initial levels (Figure 5C, black line). Strikingly, labeled RBCs in macrophage-specific GOF *Piezo1* mice declined significantly faster than in wild type and decreased to almost undetectable levels by the end of the three-week period (Figure 5C, blue line). Labeled RBCs had a half-life of about 20 days in adult wild-type mice compared to 10 days in macrophage-specific GOF *Piezo1* mice (Figure S4A). Our *in vivo* RBC turnover analysis indicates that macrophages with overactive PIEZO1 recycle more RBCs over a given time period. Indeed, we found that splenic macrophages (F4/80+) from macrophage-specific GOF *Piezo1* mice contained significantly higher amounts of intracellular RBCs (Ter119+) than wild type (Q2 in Figure 5D–E), suggesting that macrophages with GOF PIEZO1 have an increased RBC phagocytic activity *in vivo*. As expected, we observed an increase in total TER-119 positive cells (Q2 + Q3 in Figure 5D) since spleen is an important site for stress erythropoiesis in mice and TER-119 also labels erythroid progenitors (Paulson et al, 2011).

Then, we directly tested whether macrophages with overactive PIEZO1 have enhanced phagocytosis activity. We cultured bone marrow-derived macrophages from wild-type and macrophage-specific GOF *Piezo1* mice, and incubated them with fluorescent zymosan particles, a protein-carbohydrate complex from yeast cell walls that triggers phagocytosis and is engulfed by macrophages (Figure S4B). We found that fluorescence intensity (normalized to cell number) within GOF *Piezo1* macrophages was significantly higher than within wild-type macrophages (Figure 5F and Figure S4B), suggesting that overactive PIEZO1 activity enhances general phagocytosis process. To test whether overactive PIEZO1 increases phagocytosis of RBCs specifically (hemophagocytosis), we used a quantitative assay to measure phagocytic activity for opsonized RBCs. We observed a significant increase in phagocytosed RBC antigens in macrophages with GOF PIEZO1 (Figure 5G), consistent with *in vivo* data that overactive PIEZO1 in macrophages increases hemophagocytosis (Figure 5D–E).

Calcium signaling is important in phagocytosis (Nunes and Demaurex, 2010; Gronski et al., 2009). Since activated PIEZO1 conducts calcium, we hypothesized that GOF PIEZO1 induces larger intracellular calcium influx in macrophages compared to wild type. Indeed, Yoda1, a PIEZO1 specific agonist, induced larger calcium transients in macrophages with GOF PIEZO1 (Figure S4C). Rac1, a small GTPase that can be activated by calcium (Cook-Mills et al., 2004), is crucial for phagocytosis via regulating cytoskeletal organization (Mao and Finnemann, 2015). We used a quantitative assay to measure active Rac1 in macrophages during phagocytosis (Figure S4D). We observed a significantly elevated active Rac1 levels in GOF *Piezo1* macrophages when co-cultured with opsonized RBCs (Figure 5H). Interestingly, we observed increased Rac1 activation in GOF *Piezo1* macrophages before enhanced phagocytosis (compare time courses in Figure 5G and 5H), suggesting that increased Rac1 activity could cause the increased phagocytosis. Further, immunocytochemistry with a validated antibody against active Rac1 (Figure S4E) showed a similar elevation in active Rac1 in GOF *Piezo1* macrophages during phagocytosis (Figure 5I). Therefore, our data provides a potential mechanism of how excessive mechanotransduction in macrophages affects phagocytosis via calcium and Rac1 activation.

To evaluate how overactive PIEZO1 might also affect other macrophage phenotypes *in vivo*, we first examined developmental trajectory of GOF *Piezo1* macrophages. We found no significant changes for cell surface markers that define different types of macrophages (Figure S5A), suggesting that GOF PIEZO1 is unlikely to change macrophage development in a dramatic way. Further, we examined gene expression of key cytokines and interleukins in splenic macrophages and did not identify obvious changes between wild type and macrophage-specific GOF *Piezo1* mice (Figure S5B). Consistently, we did not observe a change in inflammatory molecules in the serum of macrophage-specific GOF *Piezo1* mice (Figure S5C). Together, these data suggest that overactive PIEZO1 in macrophages can increase erythrocyte turnover as a direct result of enhanced hemophagocytosis.

PIEZO1 in macrophages is required for normal response to iron stress and phagocytosis

We have established that overactive PIEZO1 in macrophages causes increased phagocytosis and reduced response to acute iron stress. However, this data does not directly address

whether endogenous PIEZO1 is involved in these processes. To assess the *in vivo* requirement of PIEZO1 in iron homeostasis, we analyzed macrophage-specific loss-of function (LOF) *Piezo1* mice. First, we showed that the majority of mechanically activated currents in macrophages depended on PIEZO1 (Figure S6A–D), suggesting that PIEZO1 is the primary mechanosensor in these cells. Next, we assessed the physiological response to short-term iron stress in these mice. We intraperitoneally injected iron dextran into adult mice at 80μg/gram body weight per day for 5 consecutive days to ensure systemic elevation of iron levels in wild-type controls (compare to Figure 4). Indeed, this short-term treatment effectively elevated serum iron level, transferrin saturation, and ferritin concentration in wild-type mice, compared to the dextran-only vehicle control (Figure 6A–C). In contrast, macrophage-specific LOF *Piezo1* mice had normal serum iron measurements and were indistinguishable from vehicle control (Figure 6A–C). This indicates that PIEZO1 is required in macrophages for physiological responses to short-term iron stress. We next examined hepcidin expression in macrophage-specific LOF *Piezo1* mice. As expected, hepcidin gene expression in the liver and serum protein levels were more robustly elevated in adult macrophage-specific LOF *Piezo1* mice after iron stress compared to wild type (Figure S6E–F). Taken together with our results from GOF *Piezo1* mice, LOF *Piezo1* data suggest that this mechanically activated channel regulates iron homeostasis by controlling hepcidin levels through a macrophage-dependent mechanism.

Examination of GOF *Piezo1* mice suggests the involvement of this channel in RBC recycling and phagocytosis by macrophages. To test whether PIEZO1 is required for these processes, we performed *in vivo* RBC turnover experiments on macrophage-specific LOF *Piezo1* mice (Figure S4A). We found that the rate of decline in fluorescence signals from macrophage-specific LOF *Piezo1* mice was significantly reduced compared to wildtype (Figure 6D), the opposite effect observed in GOF *Piezo1* mice. Indeed, RBC half-life in macrophage-specific LOF *Piezo1* mice was significantly longer than wild type (Figure S6G). Finally, we tested the requirement of PIEZO1 for macrophage phagocytosis in cultured BMDMs. Interestingly, we observed a significant reduction in internalized zymosan fluorescence in LOF *Piezo1* macrophages compared to wild-type macrophages (Figure 6E and F), indicating that PIEZO1 is required for efficient phagocytosis. In addition, we detected a reduction in intracellular RBC antigen in LOF *Piezo1* macrophages in the hemophagocytosis assay (Figure 6G), suggesting that PIEZO1 is required for efficient phagocytosis for RBCs. Importantly, we found that active Rac1 level in LOF *Piezo1* macrophages was significantly reduced during hemophagocytosis (Figure 6H), indicating that PIEZO1 regulates hemophagocytosis via Rac1 activation. These LOF data demonstrate that PIEZO1 is an essential regulator of macrophage phagocytosis and RBC recycling *in vivo*.

LOF *Piezo1* mice have no PIEZO1 expression throughout development. To test if acute inhibition of PIEZO1 can affect iron metabolism, we used GsMTX4, a non-specific inhibitor of PIEZO1 *in vitro* and *in vivo* (Bae et al., 2011; Bowman et al., 2007; Romac et al., 2018). Specifically, we tested its ability to rescue iron overload in GOF *Piezo1* mice. Remarkably, a single intraperitoneal administration of GxMTX4 (at 540ug per kg body weight) prevented serum iron elevation in response to acute iron stress (Figure S6H). These data argue against the possibility that developmental consequences of expressing GOF PIEZO1 is responsible

for the defects in iron metabolism that we observe. In addition, it raises the possibility that modulating PIEZO1 levels might be of therapeutic value. A summary of how GOF *Piezo1* mice develop iron overload is shown in Figure S6I.

E756del gain-of-function *PIEZO1* allele is associated with higher serum iron in an African American cohort.

We recently discovered a mild GOF *PIEZO1* allele (E756del) common in individuals of African descent from disparate geographic locations, with a mean allele frequency of 18% from available databases (Ma et al., 2018). Thus, an estimated up to one third of people of west African descent carry one or two copies of this allele. Because the strong but rare GOF *PIEZO1* mutations (~120 patients known worldwide) cause high serum iron levels and lead to iron overload in HX patients of European ancestry, we asked if E756del is associated with higher serum iron levels in African American carriers from the general population. To evaluate the association, we assessed serum samples from 333 self-identifying African-American individuals from two commercial blood collection centers. Individuals in this cohort are between 18 – 76 years old and the majority (85.3%) are males. They all tested negative for infectious diseases and self-reported to be healthy before blood collection. The frequency of E756del allele in this cohort was as expected (Nguetse et al., 2019; Rooks et al., 2019; Ilboudo et al., 2018): 224 individuals were non-carriers (67.3%); 101, heterozygous carriers (30.3%); and 8, homozygous carriers (2.4%).

E756del heterozygous carriers under 40-year-old did not have significantly different transferrin saturation and ferritin concentration levels compared to non-carriers within the same age group (Figure 7A). Remarkably, E756del heterozygous individuals over 40 years old had a statistically significant increase in transferrin saturation and ferritin concentrations compared to non-carriers within the same age group (Figure 7A). We observed a clear positive correlation between age and transferrin saturation/ferritin concentration in heterozygous E756del carriers, but not in non-carriers (Figure 7B). Statistical analysis was not feasible with the homozygous E756del carriers in our cohort as sample sizes were too small; however, all homozygotes had relatively elevated serum iron parameters and showed age-dependence as well (Figure 7B). These data suggest that E756del is associated with higher transferrin saturation and serum ferritin concentration in an age-dependent manner, and parallel previous work in the rare HX patients (Picard et al., 2019).

In our transgenic mouse models, we showed that hepcidin down-regulation is a mechanistic link between GOF PIEZO1 and iron overload. In the human cohorts, we found that serum hepcidin protein concentrations were significantly reduced in E756del carriers over 40 years old, compared to the non-carriers within the same age group (Figure S7A). Importantly, hepcidin levels were mildly but significantly reduced in E756del carriers under 40-year old compared to non-carriers (Figure S7A). Also, we observed an age-dependent hepcidin decline in E756del carriers (Figure S7B). This dovetails nicely with our animal model data and suggests that mild hepcidin down-regulation precedes the development of abnormally high transferrin saturation and ferritin concentration in individuals with E756del. Importantly, it shows correlation between GOF PIEZO1 data from humans and mice. Together, serum iron analysis and hepcidin measurements suggest that the biological effects

of GOF PIEZO1 on serum iron status not only apply to rare instances in individuals of European ancestry (HX patients) but also to African American individuals that self-report to be healthy.

A critical function of blood iron tests is to identify high-risk individuals that are candidates for further MRI examination. Men with > 50% and women with > 45% transferrin saturation are considered to have high transferrin saturation; while men with > 300μg/L and women with > 200 μg/L are considered to have high serum ferritin (Adams et al., 2005). Individuals with these high levels are provisionally diagnosed to have iron overload and recommended for MRI. Previous surveys have shown that about 5% of African-American individuals have high transferrin saturation and about 10% have high serum ferritin concentration (Adams et al, 2005). We applied these criteria to our cohort and found that, 6% individuals (20/333) had high transferrin saturation and 18% (60/333) had high serum ferritin concentration. We plotted the frequency distribution as well as the percentage of E756del allele against transferrin saturation and ferritin concentrations to evaluate whether E756del allele is linked to clinically high serum iron measurements (Figure S7C–D, and Figure 7C). Strikingly, although only 1 in 3 people in this cohort carry E756del, the majority of individuals with high transferrin saturation or ferritin concentrations carried at least one copy of E756del GOF *PIEZO1* (Figure 7C, right of dashed line). Indeed, 80% (16/20) of individuals with high transferrin saturation and 82% (49/60) with high serum ferritin were E756del carriers (Figure 7D). Remarkably, all individuals (10/10) with high values in both measurements were E756del carriers (Figure 7D, right panel).

Discussion

The unexplained iron overload in rare hereditary xerocytosis (HX) patients with GOF *PIEZO1* mutations (Picard et al., 2019) presented an opportunity to explore the role of mechanotransduction in iron metabolism. Our mouse genetics studies revealed an unexpected role of PIEZO1-dependent mechanotransduction in regulating erythropoiesis, macrophage phagocytosis and iron metabolism. We also highlight the relevance of our findings in a population of African Americans. We show that a common but relatively mild GOF human *PIEZO1* allele present in people of African descent is strongly associated with elevated plasma iron levels. Our work suggests that PIEZO1, a mechanically activated ion channel, is an important genetic factor involved in iron metabolism in individuals of non-European ancestry.

Macrophage mechanotransduction in iron metabolism and beyond

HX patients with GOF *PIEZO1* mutations develop age-onset iron overload in addition to RBC dehydration. Remarkably, GOF PIEZO1 expression in mouse macrophages, but not RBCs, was sufficient to induce iron overload. Results from both LOF and GOF *Piezo1* mice suggest that mechanotransduction is a key regulator of macrophage phagocytosis. For example, expression of GOF PIEZO1 in myeloid cells including macrophages induces increased turnover of RBCs. Our hypothesis is that long-term enhancement of macrophage phagocytosis impairs hepcidin production via increased erythropoiesis and erythroferrone hormone secretion, and eventually causes iron overload. Although our data is consistent with

the hypothesis that chronic decrease in hepcidin pathway by GOF PIEZO1 during adulthood causes late onset iron overload, we cannot rule out the possibility that aging processes could exacerbate disruption in iron metabolism in mice and humans. Our LOF and GOF mice studies indicate that macrophages are a key agent of PIEZO1 function in iron metabolism, but additional cell types such as RBCs and hepatocytes (Andolfo et al., 2020) as well as other myeloid cells can also be involved.

Phagocytosis by macrophages or other phagocytosing immune cells is fundamental for innate immunity and homeostasis. Previous work has focused on characterizing receptor-mediated chemical pathways in phagocytosis, but the role of mechanosensation in phagocytosis is unclear. It is easy to imagine how the act of contacting, enveloping, and internalizing pathogens or cells would depend on sensing physical forces (Jain et al., 2019). Interestingly, increased membrane tension has been shown to promote protrusion during phagocytosis (Masters et al., 2013), but how this mechanical force is converted to biological signals is still unclear. Here we show that PIEZO1, as a sensor for membrane tension, regulates downstream calcium signals and Rac1 activation during phagocytosis. PIEZO1 can be activated by macrophage/RBC interaction during phagocytosis. Alternatively, forces generated by macrophage movement or cell shape change can also be relevant. A mechanistic understanding of the role of PIEZO1 in macrophages will bring a new perspective to basic understanding of phagocytosis, as well as immune disorders with dysregulated phagocytosis. For example, our finding that macrophages with overactive PIEZO1 cause higher RBC turnover rate is reminiscent of hemophagocytosis, a common feature observed in systemic sepsis and macrophage activation syndrome (MAS; Crayne et al., 2019). Intriguingly, elevation in serum ferritin level is a reliable clinical hallmark of severe inflammation diseases like MAS.

The potential impact of our work on macrophage biology might go beyond phagocytosis and iron overload. Macrophages are a heterogeneous cell type that play varied roles in nearly all tissues. Several studies have examined the role of macrophages in tissues that experience a great deal of mechanical force. For example, PIEZO1-dependent mechanosensation is important for innate immune functions (Solis et al., 2019; Aykut et al., 2020). In addition, cardiac macrophages facilitate electrical conduction in heart (Hulsmans et al., 2017), synovial macrophages provide protective barriers for joints (Culemann et al., 2019); and tumor-associated macrophages affect cancer survival (Steidl et al., 2012). As different tissues experience distinct physical stimuli, mechanotransduction may be an important cue in shaping the physiological niche of macrophage subtypes, as is already shown for growth factors, pathogen associated molecular patterns and other chemical cues.

PIEZO1 E756del as a genetic factor that contributes to higher serum iron levels in an African American population

The genetic roots of iron overload are incompletely understood. Genome-wide association studies (GWAS) have recently identified genes in addition to *HFE* that may be involved in iron overload (Benyamin et al., 2014). Yet single-nucleotide polymorphism (SNP) based GWAS approaches often miss non-SNP variants compared to whole genome or exome studies (Tam et al., 2019), and these new approaches have not yet been thoroughly utilized

for iron disorders. Importantly, genetic factors for iron overload in populations of non-European ancestry still remain unknown.

Here, we uncovered that E756del GOF *PIEZO1* is a genetic locus associated with elevated serum iron levels in African Americans. For example, we show that 80% of high transferrin saturation and 82% of high ferritin in our cohort of African American individuals can be attributed to the presence of E756del. Furthermore, among the over 40 year-old age group in this cohort, individuals with E756del are 11.9 times more likely to have abnormally high ferritin levels compared to non-carriers (odds ratio: 12.9 95% CI: 6.3 to 26.4). We note that E756del carriers appear to have milder serum iron abnormalities when compared to HX patients: 7 out of 126 rare HX patients have serum ferritin concentration over 1000μg/L, whereas only 1 out of 109 E756del carriers in our cohort have a similarly high value. This result is expected since the very common E756del is a milder GOF allele compared to GOF *PIEZO1* mutations in HX patients (Ma et al., 2018; Albuisson et al., 2013). Strikingly, we found that ~3% of African American individuals in our cohort have both high transferrin saturation and high serum ferritin and all of these individuals are E756del carriers. Furthermore, although our cohort includes only 8 homozygous E756del carriers, we observed that E756del homozygosity may have a greater association with high serum iron levels (e.g 6/8 have high ferritin levels). Since serum ferritin and transferrin saturation are indicators for iron store, our human data clearly shows that E756del alters iron status. It is important to note that serum iron measurements are only provisional criteria for iron overload; examination of non-specific symptoms and MRI are necessary to clinically evaluate the disease penetrance of iron overload. Indeed, we expect that larger clinical studies would be important to evaluate the impact of carrying the common E756del allele for the diagnosis and perhaps the treatment of iron overload in individuals of African descent.

The role of E756del allele beyond iron overload

A recent study found that heterozygous E756del is associated with resistance to severe malaria in Gabonese children (Nguetse et al., 2019), providing epidemiological support for our previous finding on E756del allele and its role in protection from *Plasmodium* infection in mice (Ma et al., 2018). It is possible that E756del is positively selected for its role in protection against malaria (Ma et al., 2018; Nguetse et al., 2019), and that the high serum iron measurements in our cohort is a potentially deleterious consequence of carrying this allele. Interestingly, GOF PIEZO1 in macrophages did not affect malaria infection in mice (Ma et al., 2018). It seems that enhanced hemophagocytic activity is not sufficient to eliminate *Plasmodium* infected RBCs in GOF *Piezo1* mice. *Plasmodium* parasites infect reticulocytes in addition to mature RBCs. Thus, it is also possible that increased reticulocytes in GOF *Piezo1* mice, due to increased erythropoiesis, provide extra host cells for the parasites. It is, however, unlikely that altered iron levels contribute to malaria resistance in children since increased serum iron is late-onset. One limitation of our study is that we are unable to evaluate other health conditions associated with high serum iron levels in *PIEZO1* E756del carriers. As E756del is not currently genotyped in GWAS studies and is very difficult to impute (Buniello et al., 2019), large databases that associate health-related phenotypes with genome- or exome-wide sequence and that include individuals of African

descent are required to address this important question (Gurdasani et al., 2015; Ma et al., 2018).

Conclusion

Our strategy of selecting phenotypes in rare HX patients and elucidating mechanisms in transgenic mouse models has revealed an unexpected physiological relevance of mechanotransduction that goes beyond well-characterized mechanotransduction processes in physiology. Importantly, study of individuals carrying the E756del GOF *PIEZO1* common allele translates our mechanistic understanding of mechanobiology into clinically relevant insights applicable to medically under-appreciated populations. Therefore, our research provides a roadmap to use rich genomic information on *PIEZO1* to explore how mechanotransduction contributes to human physiology and disease in unexpected ways.

STAR Methods

Resource Availability

Lead Contact—Further information and requests for resources and reagents should be directed to the Lead Contact, Ardem Patapoutian (ardem@scripps.edu).

Materials Availability

Gain-of-function (GOF) *Piezo1* mice will be made available on request, but we may require a payment and/or a completed Materials Transfer Agreement.

Data and Code Availability

This study did not generate any unique datasets or code.

Experimental Model and Subject Details

Animals—All animal procedures were approved by the Institutional Animal Care and Use Committees of The Scripps Research Institute (TSRI). All animals were housed in the same vivarium conditions at a constant temperature of 20^{o}C, with a 12 hour light/dark cycle.

Constitutive, RBC-specific, and macrophage specific GOF *Piezo1* mice were generated by breeding mice with conditional GOF *Piezo1* allele with Cmv-cre (The Jackson Laboratory stock# 006054), EpoR-cre (a gift from Dr. Klingmuller group at Max-Planck-Institute für Immunbiologie, Freiburg, Germany), and LysM-cre (The Jackson Laboratory stock# 004781). All GOF *Piezo1* mice were generated at Taconic, Hudson, NY, and maintained on C57BL/6 background (Ma et al., 2018). Heterozygous GOF mice were used for the experiments, unless mentioned otherwise. Macrophage-specific LOF *Piezo1* mice were generated by breeding mice with conditional LOF Piezo1 allele (The Jackson Laboratory stock# 029213) with the same LysM-cre. All cre driver mice were on C57BL/6 background or were backcrossed at least 10 generations to C57BL/6. Littermates with a mix of equal number of male and female mice were used for experiments. Aging mice (12months to 18months old) born from same breeders were used in the experiments.

Human Subjects—Our experiments with human blood samples were approved by Institutional Review Board (IRB) at the office for the Protection of Research Subjects of Scrips Research (IRB-16–6877). Informed consent was waived for excess samples. Samples were collected from Biological Specialty Corporation (Colmar, PA) and Lampire Biological Laboratories (Pipersville, PA), approved by institutional regulations. Blood donors in this cohort are between 18 – 76 years old and the majority (85.3%) are males. Sex and age information are reported in Results. They all tested negative for infectious diseases and self-reported to be healthy before blood collection.

Method Details

Histology—Histological analysis for tissue iron accumulation was performed by Iron Stain Kit (Prussian Blue stain) from Abcam (ab150674, Cambridge, UK) according to manufacturer's instructions. Briefly, 10 μm paraffin-embedded liver sections were prepared and deparaffinized as well as dehydrated. Then sections were incubated 3 min in iron stain solution (a mixture of potassium ferrocyanide and hydrochloric acid), followed by water rinsing and counterstaining with nuclear fast and H&E. The iron in the tissues reacted with acid ferrocyanide, resulting in a blue color. Light microcopy was used to capture images (Keyence, Japan).

Serum iron Concentration measurements—Total iron was measured by Iron Assay Kit (MAK025, Sigma-Aldrich, St. Louis, MO). Briefly, whole blood was collected from mouse by cardiac puncture and serum was prepared by centrifugation. Serum was stored at −80C before experiments. Serum (5 – 10 fold dilution) was added directly to the transparent 96-well plate for chemical reaction. In the well, iron from the serum (5 – 10 fold dilution) was released by the addition of acidic buffer and reduced Fe^{3+} to Fe^{2+}. Released iron was then reacted with a chromagen that can produce a colorimetric (at 593 nm) product, proportional to the total iron level. Standard curves were prepared using iron solutions provided by the kit. The blank background for the assay is the colorimetric reading for the iron solution and blank was subtracted from all readings. Total iron concentrations were determined from the standard curve. For measuring liver iron contents, mouse livers were homogenized using Liberase (Sigma-Aldrich, St. Louis, MO) followed by treatment with Cell Lysis Buffer (Cell Signaling Technology, Danvers, MA). Cell extracts were added into transparent 96-well plates for iron assay as described above. All colorimetric readings were taken by Cytation 5 multi-mode plate reader (BioTek, Winooski, VT).

Transferrin saturation—Transferrin saturation for mouse and human serum were measured by Total Iron-Bind Capacity (TIBC) kit (BioVision, K392–100; Milpitas, CA). This assay measures TIBC and serum iron level and the transferrin saturation was calculated as percentage of serum iron level compared to TIBC. For the experiment, serum transferrin was first over-saturated with an excess amount of iron (step 1), then the unbound iron was eliminated by forming a complex with ferrozine. To measure TIBC value, iron dissociated from transferrin by changing pH was reacted with ferrozine again (step 2), and the difference in absorbance at 570 nm between step 1 and 2 reflects the capacity of total iron binding. Serum iron was also measured by a similar method as "Serum iron concentration measurements" as above. In both assays, the standard curve for iron concentration was

prepared by the iron solution with known concentration provided by the kit. Genotypes were blinded to the experimenter.

Mouse ferritin measurement—Mouse serum ferritin concentration was measured by Mouse Ferritin ELISA kit (Abcam, ab157713, Cambridge, UK). Briefly, 100 μl standard ferritin solutions and diluted serum samples (5–10 fold) were added into pre-coated wells of microtiter plates. The plates were incubated overnight in cold room (4°C), with gentle shaking. Then the plates were incubated with 100 μl 1x Enzyme-Antibody Conjugate within after extensive washing (4 times), 15 min at room temperature. Finally, stop solution was added to terminate the reaction. The absorbance at 450 nm was determined for each well by Cytation 5 multi-mode plate reader (BioTek, Winooski, VT). The experiment was performed by duplicate and averaged values were used for calculation. The mean standard readings were plotted against their concentrations to prepare the 4PL exponential sigmoidal standard curve. Ferritin protein concentrations from serum samples were then extrapolated from this curve.

Mouse whole blood count analysis—Mouse blood was collected from cardiac puncture into heparin pre-coated microtubes. 80ul fresh blood was used within one hour after collection. The analysis was performed with ProCyte Dx Hematology Analyzer (IDEXX, Westbrook, ME) by following manufacture instructions.

Mouse serum hepcidin protein measurement—Mouse serum hepcidin protein concentration was measured by HEPCIDIN ELISA kit (mouse) (Aviva Systems Biology, OKEH01408, San Diego, CA). A protocol similar to “Mouse ferritin measurement” was used with following modification: pre-coated plates were incubated with mouse serum samples at 37°C for 4 hours. After extensive washing, the plates were incubated at 37° for one hour with gentle shaking. Then, substrate solution was incubated at 37°C for 15 min. Absorbance was read at 450nm by Cytation 5 multi-mode plate reader (BioTek, Winooski, VT). The experiment was performed by duplicate and averaged values were used for calculation. The mean standard readings were plotted against their concentrations to prepare the 4PL exponential sigmoidal standard curve. Hepcidin protein concentrations from serum samples were then extrapolated from this curve.

Mouse serum erythroferrone protein measurement—Mouse serum erythroferrone concentration was measured by Mouse Erythroferrone ELISA Kit (Intrinsic LifeSciences, La Jolla, CA). Briefly, erythroferrone standard and 1:10 diluted mouse serum was incubated in the microwell assay plate for one hour at room temperature. Biotin conjugate and HRP conjugate were subsequently incubated in the plate for one hour and 30 minutes, respectively. TMB Substrate was then used to develop the color by incubating with the plate for precisely 15 minutes at room temperature. Absorbance at 450nm was measured after Stop Solution treatment. Sufficient washes were performed between each step. For data analysis, a standard curve was prepared by using Graphpad Prism 4-PL curve fit function. The protein concentration was then interpolated from the OD reading.

Iron challenge experiments—For GOF *Piezo1* mice, adult animals (2–5 months old) were intraperitoneally injected with iron dextran (Sigma-Aldrich, D8517, St. Louis, MO) at

40 μg/ gram body weight in adult mice (Zhang et al., 2011). After 18 to 24 hours, whole blood was collected from cardiac puncture to prepare serum for enzymatic assays (described above). For LOF *Piezo1* mice, adult animals (2–5 months old) were intraperitoneally injected with iron dextran at 80 μg/ gram body weight in adult mice for a consecutive 5-day period. In both experiments, dextran solution was used as a vehicle control. For GsMTX4 rescue experiment, iron challenge treatment was performed 1 hour after a single dose of GsMTX4 (Abcam, Cambridge, UK) at 540ug per kg body weight was intraperitoneally injected into mice.

***In vivo* red blood cell (RBC) clearance assay—**Whole blood was collected by cardiac puncture from C57BL/6 donor mice. RBCs were washed in sterile saline three times after centrifugation at 1000xg for 3min and then labeled with fluorescence by incubating with 5(6)-CFSE dyes (Molecular Probes C1157, Eugen, OR) at 37°C for 15–30 min. Then labeled RBCs were washed in sterile saline three times again at 1000xg for 3 min and diluted to 5×10^5 RBCs/ml as working solution. 200 μl working solution was intravenously injected into the tail veins of experimental mice for analysis. Every three days, 1.5–2 μl tail blood was collected from injected mice in 180 μl Dulbecco's Phosphate Buffer Solution with 2% fetal bovine serum on 96-well plates. The cytometry was performed with NovoCyte Flow Cytometry system (ACEA Biosciences, San Diego CA) following manufacturer's instruction. Briefly, erythrocytes were selected by gating on forward/side-light scatter. Fluorescence was measured by excitation of RBCs with a laser at a wavelength of 488 nm and emission of the green fluorescence for CFSE probe. We analyzed RBC fluorescence intensity in experiments comparing wild-type and GOF mice immediately after collecting tail blood each day (Figure 5). However, we had limited access to the cytometry facility during the partial shutdown of Scripps Research during COVID19 pandemic. Therefore, when performing similar RBC fluorescence assay on wild-type and LOF littermates, we fixed and saved the tail blood samples at various timepoints at 4°C for up to 7 days before analysis. This could explain the small difference in half-life values of wild-type mice in GOF and LOF experiments (Figure 5C and Figure S4C).

Flow cytometry—Adult mice between 2–6 months old were sacrificed by CO_2 inhalation. Spleens were dissected from abdomen and cells were filtered through 70μm nylon strainer (Corning Falcon, Tewksbury, MA). Erythrocytes were lysed by 1xRBC lysis buffer (Biolegend, San Diego, CA). A single splenic cell suspension was then obtained. Antibodies for FACS sorting were used to stain splenic cells: AF647-conjugated F4/80 (pan-macrophages), Alexa 488-conjugated CD68 (M1 macrophages), PE-Dazzle 594-conjugated CD86 (M1 macrophages), PE-conjugated CD163 (M2 macrophages), BV711-conjugated MHC-II (MHC-II macrophages), eFluor450-conjugated CD3, CD19, NK1.1 (for excluding T-, B- and NK- cells) and BV421-conjugated TER119 (erythrocyte). Antibodies were purchased from Biolegend and used at recommended concentration by manufacture. Briefly, surface protein markers were stained on ice followed by fixation/permeabilization at room temperature. Then, antibody for intracellular antigen (TER-119) was used to stain the cells at room temperature. FACS sorting was performed on Yeti model ZE5 Bio-Rad (Irvine, CA) at Flow core facility of Scripps Research. Briefly, dead cells (NIR Zombie stain, Biolegend) as well as T-, B- and NK-cells were excluded. F4/80 positive cells were further analyzed for

M1 and M2 macrophages. To evaluate hemophagocytosis, F4/80 and Ter-119 double positive cells were counted. Unstained cells were used as a negative to for cytometry. Data were analyzed by FlowJO (BD Biosciences, San Diego, CA). For gene expression experiment of splenic macrophages, F4/80 positive cells were collected directly in TRIzol solution for RNA preparation (see below).

Macrophage phagocytosis assay—Macrophages were cultured from bone marrow blood progenitor cells following a well-established protocol (Weischenfeldt and Porse, 2008). Briefly, bone marrow cells were isolated from adult mouse femur with lymphocyte medium (RPMI-1640 + 10% fetal bovine serum) and cultured with the presence of 10 ng/ml mouse colony stimulating factor (mCSF) for 6–8 days at 37°C before experiments. For general *in vitro* phagocytosis assay using zymosan particles, macrophages were starved with lymphocyte medium (without mCSF) for 2 hours. Then, 5 μL of fluorescent zymosan particles were incubated with the starved macrophages for 2 hours at 37°C. To quantify the phagocytosis, cells were washed by PBS three times with DAPI staining in the last wash for 20 min at room temperature. Then cells were fixed and imaged using mCherry and DAPI channels on fluorescence microscope (Keyence, Japan). The fluorescence intensities from macrophages were normalized to DAPI positive cells to represent phagocytosis activity. For hemophagocytosis assay, starved wild type, GOF and LOF *Piezo1* macrophages (prepared as same procedure above) were incubated with opsonized RBCs with reagents from CytoSelect 96-Well Phagocytosis Assay (RBC substrate, Cell Biolabs, CBA-220). Cells at different time courses during phagocytosis were collected and lysed for quantifying RBC content by measuring the absorbance at 610nm (Cell Biolabs, San Diego, CA).

Calcium imaging experiments.: Experiments performed by a previously published procedure (Ma et al., 2018). Briefly, bone marrow derived macrophages (BMDMs) were cultured from wild type, GOF and LOF *Piezo1* mice as described above. To measure calcium signals, BMDMs were seeded into 384-well reader plate, at 20,000 cells per well. The plate was incubated overnight then washed with assay buffer (1xHBSS, 10mM HEPES, pH7.4). During imaging, Yoda1 (Fisher Scientific, Waltham, MA) was added into the reader plate in a serially diluted manner. Intracellular calcium was measured by Fluo-8 AM dye (Fisher Scientific, Waltham, MA) pre-loaded into BMDMs. Time zero was the time point of initial Yoda1 addition and the calcium signal at time zero was defined as zero. All data points were normalized to time zero.

Rac1 activation assay and immunocytochemistry.: To validate this assay, mouse embryonic fibroblasts (MEFs) were treated with 10ng/ml epidermal growth factor (EGF, Sigma-Aldrich, St. Louis, MO) for 15minutes. Then, MEFs were lysed and active Rac1 levels were measured by Rac1G-LISA Activation Assay Kit (enzyme-linked immunosorbent based assay) (Cytoskeleton Inc., Denver, CO) following manufacturer's instruction. As a control, MEFs were incubated with 10ng/ml EGF and 100uM NSC23766, a specific Rac1 inhibitor (Tocris, Minneapolis, MN). Wild type, GOF and LOF *Piezo1* BMDMs during phagocytosis (see above section on macrophage phagocytosis assay) were lysed at different time points for detecting active Rac1 protein. Time zero (before phagocytosis) is the baseline signal and defined as zero. All data were normalized to time zero. Similarly, antibody

specific for active Rac1 (1:200 dilution, NewEast Biosciences, King of Prussia, PA) was validated in MEFs by EGF and Rac1 inhibitor treatment. Wild type and GOF *Piezo1* BMDMs were fixed by 4% PFA after 30min phagocytosis followed by antibody staining. Fluorescent images were captured by a Nikon Instruments A1R+ confocal microscope.

***In situ* hybridization—**BMDMs from wild type and LOF *Piezo1* adult mice (2–6 months) were cultured on glass coverslips for 7 days. RNAscope procedures were performed according to manufacturer's instructions (ACDBio: #323100) using probes against *Piezo1* (ACDBio: #400181) and *Piezo2* (ACDBio: #439971-C2).

Real time quantitative PCR.: Total RNA was isolated from mouse livers or FACS sorted splenic macrophages by TRIzol Reagent (Thermo Fisher Scientific, Waltham, MA). At least 100 ng total RNA was used to generate 1st strand cDNA using the Quantitect reverse transcription kit (Qiagen). Real time PCR assays were set up using GoTaq qPCR Master Mix (Promega, Madison WI). The reaction was run in the ABI 7900HT fast real time system using 1 μl of the cDNA in a 20 μl reaction according to the manufacturer's instructions in triplicates. Primers were designed for target gene (m*hepcidin*) (forward GGCAAAGAGGCAAAATGTGC, reverse TTGAGCTTGCTCTGGTGTCTGG) and reference gene (*Gapdh*) (forward primer GCACCACCAACTGCTTAG, reverse primer GGATGCAGGGATGATGTTC). Il-1 beta (forward CCAGCTTCAAATCTCACAGCAG, reverse CTTCTTTGGGTATTGCTTGGGATC), Il-6 (forward TCCAGTTGCCTTCTTGGGAC, reverse GTACTCCAGAAGACCAGAGG), Il-10 (forward TGGCCCAGAAATCAAGGAGC, reverse CAGCAGACTCAATACACACT), TNFa (forward CACAGAAAGCATGATCCGCGACGT, reverse CGGCAGAGAGGAGGTTGACTTTCT), TGFbeta (forward GACCGCAACAACGCCATCTA, reverse GGCGTATCAGTGGGGGTCAG), Il12b (forward GTCCTCAGAAGCTAACCATCTCC, reverse CCAGAGCCTATGACTCCATGTC), Il-12a (forward CAATCACGCTACCTCCTCTTTT, reverse CAGCAGTGCAGGAATAATGTTTC), Il-23 (forward CAGCAGCTCTCTCGGAATCTC, reverse TGGATACGGGGCACATTATTTTT), ccl2 (forward TTAAAAACCTGGATCGGAACCAA, reverse GCATTAGCTTCAGATTTACGGGT), ccl3 (forward TGTACCATGACACTCTGCAAC, reverse CAACGATGAATTGGCGTGGAA), ccl4 (forward TTCCTGCTGTTTCTCTTACACCT, reverse CTGTCTGCCTCTTTTGGTCAG), ccl5 (forward GCTGCTTTGCCTACCTCTCC, reverse TCGAGTGACAAACACGACTGC), ccl17 (forward TACCATGAGGTCACTTCAGATGC, reverse GCACTCTCGGCCTACATTGG), cxcl10 (forward CCAAGTGCTGCCGTCATTTTC, reverse GGCTCGCAGGGATGATTTCAA), ccl1 (forward TGCCGTGTGGATACAGGATG, reverse GTTGAGGCGCAGCTTTCTCTA). Calibrations and normalizations were done using the 2-ΔΔCT method, where ΔΔCT = ((CT(target gene) - CT (reference gene)) - (CT (calibrator) - CT (reference gene)).

Mouse inflammatory cytokines analysis.: Serum inflammatory molecules were measured by Mouse Inflammatory Cytokines Multi-Analyte ELISArray Kits (Qiagen, Hilden, Germany) according to manufacturer's instruction. Briefly, 10ul serum from wild type GOF

Piezo1 adult mice (2 – 6 months old) was used for the assay. Protein levels were measured by absorbance at 450um.

Electrophysiology for mechanotransduction in macrophages—Bone marrow cells were plated on 12 mm diameter PDL-coated coverslips on day 1 after extraction (100K cells/well in 24-well plate) from WT and macrophage KO littermates (LyzM-cre) and treated with mouse CSF recombinant protein at 10ng/mL (Gibco, Dublin, Ireland) to induce differentiated BMDMs. On day 5, cells derived from two separate experiments were tested using cell attached patch clamp methods for their responsiveness to membrane stretch using a HSPC (Coste et al., 2015; Murthy et al., 2018). LPS (20 or 50 ng/ml, 1–3 days) was used to induce membrane changes mimicking those occurring during phagocytosis. Pipettes with large diameter tips (electrodes had resistances of 1.4 – 2.6 MΩ) were needed to observe channel activity in WT BMDMs. Similar pipettes were used for recordings of WT (2.0 ± 0.3 MΩ, n=18) and LoF (2.1 ± 0.3 MΩ, n=14) cells. Cells were maintained in a high KCl bath solution during recordings to depolarize the membrane potential. Cells were tested on days 6, 7 and 8 after plating, a time when most precursors had differentiated into mature BMDMs. The final confluency was ~50%. Spontaneous single channel currents with amplitudes consistent with mouse Piezo1 (Coste et al., 2015, Fig. 2e) were often observed at a pipette potential of 80mV (during at least 30 sec of observation; membrane potential near −80mV depending on resting potential). In WT cells 11 of the 18 cells recorded revealed spontaneousz activity and, of these, 10 responded with stretch activated currents; of those having no mPiezo1-like spontaneous activity (n=7), 5 were non-responsive to stretch. In the case of the LoF cells, only 2 of 14 cells revealed spontaneous activity similar to that observed in WT cells, one of which revealed SAC (Supplemental Figure S6A–S6D). In one WT case, determination of the SAC reversal potential was possible and it was consistent with being mediated by a non-selective cation channel (−1.4mV).

Genotyping E756del carriers by sequencing—333 blood samples (less than 1 ml) were used for DNA preparation and genotyping, while serum was used for transferrin saturation, ferritin and hepcidin measurements. 200 μL of blood samples were used for genomic DNA isolation by QIAamp DNA Blood Mini Kit (Qiagen, Germany). A ~200 bp PCR amplicon that contained E756 locus was generated for sequencing E756del or wild type allele (forward primer: 5’CAGGCAGGATGCAGTGAGTG3’, reverse primer: 5’GGACATGGCACAGCAGACTG3’. Reverse primer was used for sequencing).

Human hepcidin measurement—Human serum hepcidin concentration was measured by Human Hepcidin Quantikine ELISA kit (R&D Systems, DHP250, Minneapolis, MN). Briefly, 50 μl standard hepcidin solutions and diluted serum samples (10 fold) were added into pre-coated wells of microtiter plates. The plates were incubated with 200 μl human hepcidin conjugate overnight in cold room (4°C), with gentle shaking. Then the plates were incubated with 200 μl substrate solution after extensive washing (4 times) at room temperature about 2 hours, followed by the addition of stop solution. The absorbance at 540um was determined for each well by Cytation 5 multi-mode plate reader (BioTek, Winooski, VT). The experiment was performed by duplicate and averaged values were used for calculation. The mean standard readings against their concentrations were used to

prepare the best smooth curve. Hepcidin protein concentrations from serum samples were then extrapolated from this curve. Genotypes were blinded to the experimenter.

Human ferritin measurement—Human serum ferritin concentration was measured by Human Ferritin ELISA kit (Sigma-Aldrich, RAB0197, St. Louis, MO). Briefly, 100 μL standard ferritin solutions and diluted serum samples (10-fold) were added into pre-coated wells of microtiter plates. The plates were then incubated overnight in cold room (4°C), with gentle shaking. Then the plates were incubated with 100 μL detection antibody for 1 hour after extensive washing (4 times) at room temperature. Next, 100 μL HRP-Streptavidin solution was added and incubated 45 min at room temperature. Finally, 100 μL ELISA Colorimetric was added and incubated for 30min at room temperature. The absorbance at 450um was determined for each well by Cytation 5 multi-mode plate reader (BioTek, Winooski, VT). The experiment was performed by duplicate and averaged values were used for calculation. The mean standard readings against their concentrations were used to prepare the best smooth curve. Ferritin protein concentrations from serum samples were then extrapolated from this curve. Genotypes were blinded to the experimenter.

Quantification and statistical analysis—One-way ANOVA analysis was performed for Figure 1 and Figure 2. Student t-tests (two-tail) were performed for Figure 3, Figure 5, Figure 6 and Figure 7. Multiple t-tests by Bonferroni correction were performed for Figure 4 and Figure 6. Prism 8 software was used for all statistical analyses, standard curve preparation and data visualization. Statistical details about n number and p-value are reported in Figure legends.

Supplementary Material

Refer to Web version on PubMed Central for supplementary material.

Acknowledgements

We thank Adrienne Dubin, Tomas Ganz, Rose Hill, and Kara Marshall for critical reading of the manuscript. We thank Roberto Aiolfi from Ruggeri lab at TSRI for sharing ProCyte equipment. We also thank Achille Iolascon and Roberta Russo for discussions on experimental design. This work was supported by the following grants: NIH R35 NS105067 and R01 DE022358 to A.P. S.M was supported by Calibr-GHDDI Gates postdoctoral fellowship. A.P is an investigator of the Howard Hughes Medical Institute. The authors declare no competing financial interests.

References

Adams PC, Reboussin DM, Barton JC, McLaren CE, Eckfeldt JH, McLaren GD, Dawkins FW, Acton RT, Harris EL, Gordeuk VR, et al. (2005). Hemochromatosis and iron-overload screening in a racially diverse population. N. Engl. J. Med 352, 1769–1778. [PubMed: 15858186]

Albuisson J, Murthy SE, Bandell M, Coste B, Louis-Dit-Picard H, Mathur J, Fénéant-Thibault M, Tertian G, de Jaureguiberry J-P, Syfuss P-Y, et al. (2013). Dehydrated hereditary stomatocytosis linked to gain-of-function mutations in mechanically activated PIEZO1 ion channels. Nat Commun 4, 1884. [PubMed: 23695678]

Andolfo I, Rosato BE, Manna F, De Rosa G, Marra R, Gambale A, Girelli D, Russo R, and Iolascon A (2020). Gain-of-function mutations in PIEZO1 directly impair hepatic iron metabolism via the inhibition of the BMP/SMADs pathway. Am J Hematol 95, 188–197. [PubMed: 31737919]

Andrews NC, and Ganz T (2019). The molecular basis of iron metabolism. In Molecular Hematology 4e, Provan D, and Gribben J, eds. (Wiley), pp. 161–172.

Aykut B, Chen R, Kim JI, Wu D, Shadaloey SAA, Abengozar R, Preiss P, Saxena A, Pushalkar S, Leinwand J, et al. (2020). Targeting Piezo1 unleashes innate immunity against cancer and infectious disease. Sci. Immunol 5, eabb5168.

Bae C, Sachs F, and Gottlieb PA (2011). The mechanosensitive ion channel Piezo1 is inhibited by the peptide GsMTx4. Biochemistry 50, 6295–6300. [PubMed: 21696149]

Benyamin B, Esko T, Ried JS, Radhakrishnan A, Vermeulen SH, Traglia M, Gögele M, Anderson D, Broer L, Podmore C, et al. (2014). Novel loci affecting iron homeostasis and their effects in individuals at risk for hemochromatosis. Nat Commun 5, 4926. [PubMed: 25352340]

Bowman CL, Gottlieb PA, Suchyna TM, Murphy YK, and Sachs F (2007). Mechanosensitive ion channels and the peptide inhibitor GsMTx-4: history, properties, mechanisms and pharmacology. Toxicon 49, 249–270. [PubMed: 17157345]

Brissot P, Pietrangelo A, Adams PC, de Graaff B, McLaren CE, and Loréal O (2018). Haemochromatosis. Nat Rev Dis Primers 4, 18016. [PubMed: 29620054]

Buniello A, MacArthur JAL, Cerezo M, Harris LW, Hayhurst J, Malangone C, McMahon A, Morales J, Mountjoy E, Sollis E, et al. (2019). The NHGRI-EBI GWAS Catalog of published genome-wide association studies, targeted arrays and summary statistics 2019. Nucleic Acids Res. 47, D1005–D1012. [PubMed: 30445434]

Cahalan SM, Lukacs V, Ranade SS, Chien S, Bandell M, and Patapoutian A (2015). Piezo1 links mechanical forces to red blood cell volume. Elife *4*.

Clausen BE, Burkhardt C, Reith W, Renkawitz R, and Förster I (1999). Conditional gene targeting in macrophages and granulocytes using LysMcre mice. Transgenic Res. 8, 265–277. [PubMed: 10621974]

Cook-Mills JM, Johnson JD, Deem TL, Ochi A, Wang L, and Zheng Y (2004). Calcium mobilization and Rac1 activation are required for VCAM-1 (vascular cell adhesion molecule-1) stimulation of NADPH oxidase activity. Biochem. J 378, 539–547. [PubMed: 14594451]

Coste B, Mathur J, Schmidt M, Earley TJ, Ranade S, Petrus MJ, Dubin AE, and Patapoutian A (2010). Piezo1 and Piezo2 are essential components of distinct mechanically activated cation channels. Science 330, 55–60. [PubMed: 20813920]

Crayne CB, Albeituni S, Nichols KE, and Cron RQ (2019). The Immunology of Macrophage Activation Syndrome. Front. Immunol 10, 119. [PubMed: 30774631]

Culemann S, Grüneboom A, Nicolás-Ávila JÁ, Weidner D, Lämmle KF, Rothe T, Quintana JA, Kirchner P, Krljanac B, Eberhardt M, et al. (2019). Locally renewing resident synovial macrophages provide a protective barrier for the joint. Nature 572, 670–675. [PubMed: 31391580]

Dabbagh AJ, Trenam CW, Morris CJ, and Blake DR (1993). Iron in joint inflammation. Ann. Rheum. Dis 52, 67–73. [PubMed: 8427520]

Dholakia U, Bandyopadhyay S, Hod EA, and Prestia KA (2015). Determination of RBC Survival in C57BL/6 and C57BL/6-Tg(UBC-GFP) Mice. Comp. Med 65, 196–201. [PubMed: 26141444]

Donovan A, Lima CA, Pinkus JL, Pinkus GS, Zon LI, Robine S, and Andrews NC (2005). The iron exporter ferroportin/Slc40a1 is essential for iron homeostasis. Cell Metab. 1, 191–200. [PubMed: 16054062]

Feder JN, Gnirke A, Thomas W, Tsuchihashi Z, Ruddy DA, Basava A, Dormishian F, Domingo R, Ellis MC, Fullan A, et al. (1996). A novel MHC class I-like gene is mutated in patients with hereditary haemochromatosis. Nat. Genet 13, 399–408. [PubMed: 8696333]

Fleming RE, and Ponka P (2012). Iron overload in human disease. N. Engl. J. Med 366, 348–359. [PubMed: 22276824]

Ganz T (2011). Hepcidin and iron regulation, 10 years later. Blood 117, 4425–4433. [PubMed: 21346250]

Ganz T (2012). Macrophages and systemic iron homeostasis. J Innate Immun 4, 446–453. [PubMed: 22441209]

Ganz T (2013). Systemic Iron Homeostasis. Physiological Reviews 93, 1721–1741. [PubMed: 24137020]

Ganz T, and Nemeth E (2012a). Iron metabolism: interactions with normal and disordered erythropoiesis. Cold Spring Harb Perspect Med 2, a011668.

Ganz T, and Nemeth E (2012b). Hepcidin and iron homeostasis. Biochim. Biophys. Acta 1823, 1434–1443. [PubMed: 22306005]

Gomme PT, McCann KB, and Bertolini J (2005). Transferrin: structure, function and potential therapeutic actions. Drug Discov. Today 10, 267–273. [PubMed: 15708745]

Gronski MA, Kinchen JM, Juncadella IJ, Franc NC, and Ravichandran KS (2009). An essential role for calcium flux in phagocytes for apoptotic cell engulfment and the anti-inflammatory response. Cell Death Differ. 16, 1323–1331. [PubMed: 19461656]

Gujja P, Rosing DR, Tripodi DJ, and Shizukuda Y (2010). Iron overload cardiomyopathy: better understanding of an increasing disorder. J. Am. Coll. Cardiol 56, 1001–1012. [PubMed: 20846597]

Gurdasani D, Carstensen T, Tekola-Ayele F, Pagani L, Tachmazidou I, Hatzikotoulas K, Karthikeyan S, Iles L, Pollard MO, Choudhury A, et al. (2015). The African Genome Variation Project shapes medical genetics in Africa. Nature 517, 327–332. [PubMed: 25470054]

Heinrich AC, Pelanda R, and Klingmüller U (2004). A mouse model for visualization and conditional mutations in the erythroid lineage. Blood 104, 659–666. [PubMed: 15090451]

Hershko C (2010). Pathogenesis and management of iron toxicity in thalassemia. Ann. N. Y. Acad. Sci 1202, 1–9. [PubMed: 20712765]

Hulsmans M, Clauss S, Xiao L, Aguirre AD, King KR, Hanley A, Hucker WJ, Wülfers EM, Seemann G, Courties G, et al. (2017). Macrophages Facilitate Electrical Conduction in the Heart. Cell 169, 510–522.e20.

Ilboudo Y, Bartolucci P, Garrett ME, Ashley-Koch A, Telen M, Brugnara C, Galactéros F, and Lettre G (2018). A common functional PIEZO1 deletion allele associates with red blood cell density in sickle cell disease patients. Am. J. Hematol 93, E362–E365. [PubMed: 30105803]

Jain N, Moeller J, and Vogel V (2019). Mechanobiology of Macrophages: How Physical Factors Coregulate Macrophage Plasticity and Phagocytosis. Annu. Rev. Biomed. Eng 21, 267–297. [PubMed: 31167103]

Jensen P-D (2004). Evaluation of iron overload. Br J Haematol 124, 697–711. [PubMed: 15009057]

Kautz L, Jung G, Valore EV, Rivella S, Nemeth E, and Ganz T (2014). Identification of erythroferrone as an erythroid regulator of iron metabolism. Nat Genet 46, 678–684. [PubMed: 24880340]

Kautz L, Jung G, Du X, Gabayan V, Chapman J, Nasoff M, Nemeth E, and Ganz T (2015).

Erythroferrone contributes to hepcidin suppression and iron overload in a mouse model of β-thalassemia. Blood 126, 2031–2037.

Knovich MA, Storey JA, Coffman LG, Torti SV, and Torti FM (2009). Ferritin for the clinician. Blood Rev. 23, 95–104. [PubMed: 18835072]

Korolnek T, and Hamza I (2015). Macrophages and iron trafficking at the birth and death of red cells. Blood 125, 2893–2897. [PubMed: 25778532]

Li J, Hou B, Tumova S, Muraki K, Bruns A, Ludlow MJ, Sedo A, Hyman AJ, McKeown L, Young RS, et al. (2014). Piezo1 integration of vascular architecture with physiological force. Nature 515, 279–282. [PubMed: 25119035]

Ma S, Cahalan S, LaMonte G, Grubaugh ND, Zeng W, Murthy SE, Paytas E, Gamini R, Lukacs V, Whitwam T, et al. (2018). Common PIEZO1 Allele in African Populations Causes RBC Dehydration and Attenuates Plasmodium Infection. Cell 173, 443–455.e12.

Mao Y, and Finnemann SC (2015). Regulation of phagocytosis by Rho GTPases. Small GTPases 6, 89–99. [PubMed: 25941749]

Masters TA, Pontes B, Viasnoff V, Li Y, and Gauthier NC (2013). Plasma membrane tension orchestrates membrane trafficking, cytoskeletal remodeling, and biochemical signaling during phagocytosis. Proc. Natl. Acad. Sci. U.S.A 110, 11875–11880. [PubMed: 23821745]

Milic S, Mikolasevic I, Orlic L, Devcic E, Starcevic-Cizmarevic N, Stimac D, Kapovic M, and Ristic S (2016). The Role of Iron and Iron Overload in Chronic Liver Disease. Med. Sci. Monit 22, 2144–2151. [PubMed: 27332079]

Mobarra N, Shanaki M, Ehteram H, Nasiri H, Sahmani M, Saeidi M, Goudarzi M, Pourkarim H, and Azad M (2016). A Review on Iron Chelators in Treatment of Iron Overload Syndromes. Int J Hematol Oncol Stem Cell Res 10, 239–247. [PubMed: 27928480]

Muckenthaler MU, Rivella S, Hentze MW, and Galy B (2017). A Red Carpet for Iron Metabolism. Cell 168, 344–361. [PubMed: 28129536]

Nguetse CN, Purington N, Ebel ER, Shakya B, Tetard M, Kremsner PG, Velavan TP, and Egan ES (2020). A common polymorphism in the mechanosensitive ion channel *PIEZO1* is associated with protection from severe malaria in humans. Proc Natl Acad Sci USA 117, 9074–9081. [PubMed: 32265284]

Nunes P, and Demaurex N (2010). The role of calcium signaling in phagocytosis. Journal of Leukocyte Biology 88, 57–68. [PubMed: 20400677]

Papanikolaou G, Tzilianos M, Christakis JI, Bogdanos D, Tsimirika K, MacFarlane J, Goldberg YP, Sakellaropoulos N, Ganz T, and Nemeth E (2005). Hepcidin in iron overload disorders. Blood 105, 4103–4105. [PubMed: 15671438]

Park CH, Valore EV, Waring AJ, and Ganz T (2001). Hepcidin, a urinary antimicrobial peptide synthesized in the liver. J. Biol. Chem 276, 7806–7810. [PubMed: 11113131]

Parmley RT, Spicer SS, and Alvarez CJ (1978). Ultrastructural localization of nonheme celluar iron with ferrocyanide. J. Histochem. Cytochem 26, 729–741. [PubMed: 712049]

Pasricha S-R, McHugh K, and Drakesmith H (2016). Regulation of Hepcidin by Erythropoiesis: The Story So Far. Annu. Rev. Nutr 36, 417–434. [PubMed: 27146013]

Paulson RF, Shi L, and Wu D-C (2011). Stress erythropoiesis: new signals and new stress progenitor cells. Curr. Opin. Hematol 18, 139–145. [PubMed: 21372709]

Picard V, Guitton C, Thuret I, Rose C, Bendelac L, Ghazal K, Aguilar-Martinez P, Badens C, Barro C, Bénéteau C, et al. (2019). Clinical and biological features in PIEZO1-hereditary xerocytosis and Gardos channelopathy: a retrospective series of 126 patients. Haematologica 104, 1554–1564. [PubMed: 30655378]

Pilling LC, Tamosauskaite J, Jones G, Wood AR, Jones L, Kuo C-L, Kuchel GA, Ferrucci L, and Melzer D (2019). Common conditions associated with hereditary haemochromatosis genetic variants: cohort study in UK Biobank. BMJ 364, k5222. [PubMed: 30651232]

Ranade SS, Qiu Z, Woo S-H, Hur SS, Murthy SE, Cahalan SM, Xu J, Mathur J, Bandell M, Coste B, et al. (2014). Piezo1, a mechanically activated ion channel, is required for vascular development in mice. Proc. Natl. Acad. Sci. U.S.A 111, 10347–10352. [PubMed: 24958852]

Romac JM-J, Shahid RA, Swain SM, Vigna SR, and Liddle RA (2018). Piezo1 is a mechanically activated ion channel and mediates pressure induced pancreatitis. Nat Commun 9, 1715. [PubMed: 29712913]

Rooks H, Brewin J, Gardner K, Chakravorty S, Menzel S, Hannemann A, Gibson J, and Rees DC (2019). A gain of function variant in PIEZO1 (E756del) and sickle cell disease. Haematologica 104, e91–e93. [PubMed: 30237267]

Roy CN, Penny DM, Feder JN, and Enns CA (1999). The hereditary hemochromatosis protein, HFE, specifically regulates transferrin-mediated iron uptake in HeLa cells. J. Biol. Chem 274, 9022–9028. [PubMed: 10085150]

Schwenk F, Baron U, and Rajewsky K (1995). A cre-transgenic mouse strain for the ubiquitous deletion of loxP-flanked gene segments including deletion in germ cells. Nucleic Acids Res. 23, 5080–5081. [PubMed: 8559668]

Solis AG, Bielecki P, Steach HR, Sharma L, Harman CCD, Yun S, de Zoete MR, Warnock JN, To SDF, York AG, et al. (2019). Mechanosensation of cyclical force by PIEZO1 is essential for innate immunity. Nature 573, 69–74. [PubMed: 31435009]

Steidl C, Lee T, Shah SP, Farinha P, Han G, Nayar T, Delaney A, Jones SJ, Iqbal J, Weisenburger DD, et al. (2010). Tumor-associated macrophages and survival in classic Hodgkin's lymphoma. N. Engl. J. Med 362, 875–885. [PubMed: 20220182]

Sun W, Chi S, Li Y, Ling S, Tan Y, Xu Y, Jiang F, Li J, Liu C, Zhong G, et al. (2019). The mechanosensitive Piezo1 channel is required for bone formation. ELife 8, e47454.

Tabula Muris Consortium, Overall coordination, Logistical coordination, Organ collection and processing, Library preparation and sequencing, Computational data analysis, Cell type annotation, Writing group, Supplemental text writing group, and Principal investigators (2018). Single-cell transcriptomics of 20 mouse organs creates a Tabula Muris. Nature 562, 367–372. [PubMed: 30283141]

Taher AT, and Saliba AN (2017). Iron overload in thalassemia: different organs at different rates. Hematology Am Soc Hematol Educ Program 2017, 265–271. [PubMed: 29222265]

Tam V, Patel N, Turcotte M, Bossé Y, Paré G, and Meyre D (2019). Benefits and limitations of genome-wide association studies. Nat. Rev. Genet 20, 467–484. [PubMed: 31068683]

Weischenfeldt J, and Porse B (2008). Bone Marrow-Derived Macrophages (BMM): Isolation and Applications. CSH Protoc 2008, pdb.prot5080.

Woo S-H, Lukacs V, de Nooij JC, Zaytseva D, Criddle CR, Francisco A, Jessell TM, Wilkinson KA, and Patapoutian A (2015). Piezo2 is the principal mechanotransduction channel for proprioception. Nat. Neurosci 18, 1756–1762. [PubMed: 26551544]

Zarychanski R, Schulz VP, Houston BL, Maksimova Y, Houston DS, Smith B, Rinehart J, and Gallagher PG (2012). Mutations in the mechanotransduction protein PIEZO1 are associated with hereditary xerocytosis. Blood 120, 1908–1915. [PubMed: 22529292]

Zeng W-Z, Marshall KL, Min S, Daou I, Chapleau MW, Abboud FM, Liberles SD, and Patapoutian A (2018). PIEZOs mediate neuronal sensing of blood pressure and the baroreceptor reflex. Science 362, 464–467. [PubMed: 30361375]

Zhang Z, Zhang F, An P, Guo X, Shen Y, Tao Y, Wu Q, Zhang Y, Yu Y, Ning B, et al. (2011). Ferroportin1 deficiency in mouse macrophages impairs iron homeostasis and inflammatory responses. Blood 118, 1912–1922. [PubMed: 21705499]

Highlights

- Expression of gain-of-function PIEZO1 in macrophages induces iron overload in mice
- PIEZO1 in macrophages plays an important role in regulating phagocytosis
- PIEZO1 contributes to iron overload by increasing red blood cell turnover *in vivo*
- Gain-of-function *PIEZO1* is linked to elevated serum iron in American African individuals

Gain-of-function mutations in the mechanosensitive ion channel PIEZO1 results in iron overload and interference with iron metabolism

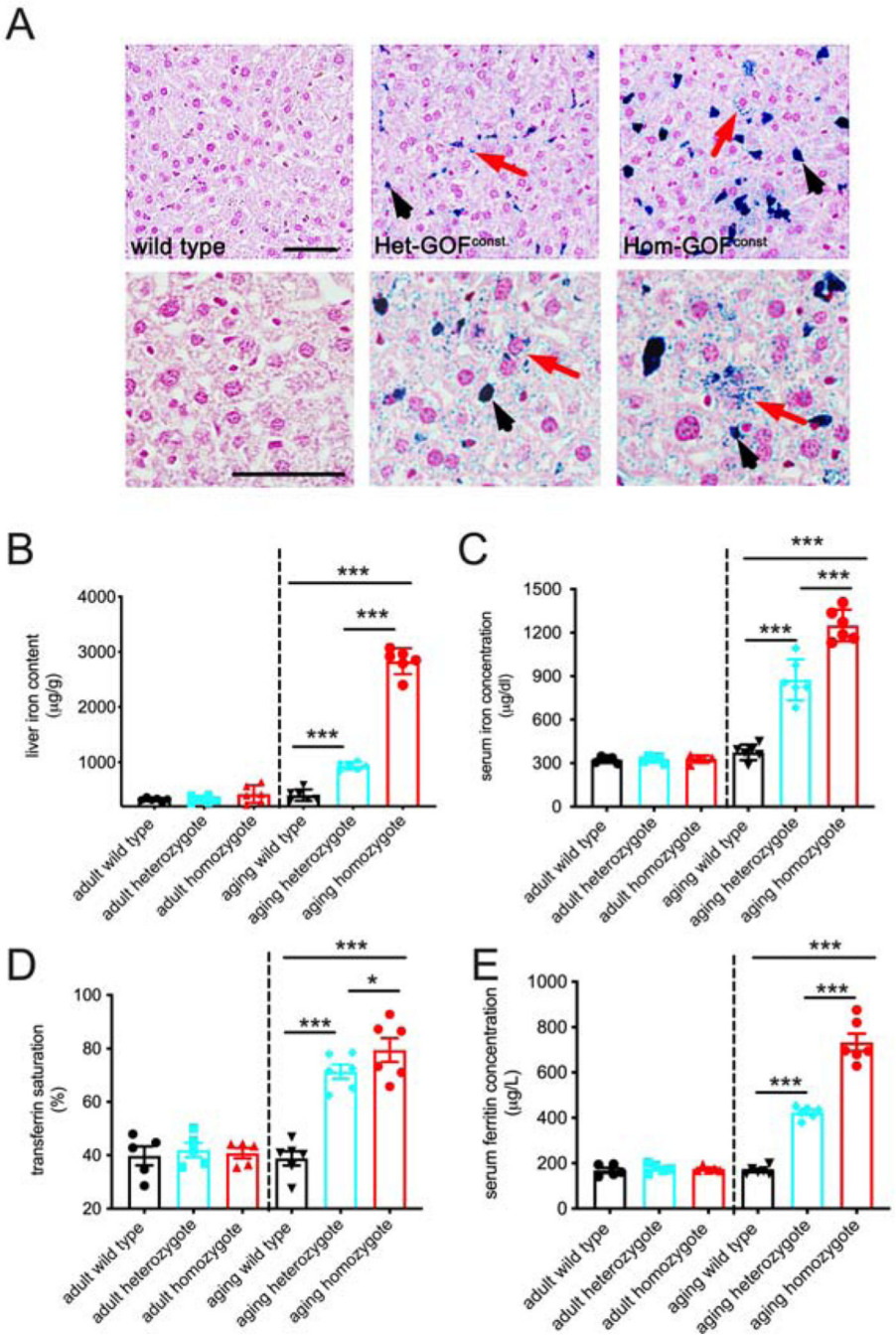

Figure 1.

Gain-of-function (GOF) *Piezo1* mice develop late-onset iron overload.

A. Perls Prussian blue staining in 10μm paraffin sections of livers from aging wild-type and constitutive GOF *Piezo1* mice (higher magnification examples shown in lower panels). Blue color represents iron staining in hepatocytes (red arrow) and Kupffer cells (black arrowhead). Note more iron staining in homozygotes compared to heterozygotes. (Hematoxylin and eosin (H&E) staining used as background. Het: heterozygote; Hom:

homozygote) Constitutive GOF mice were generated by breeding GOF mice with animals expressing a ubiquitous Cre driver (CMV-Cre). Scale bars: 50 μm.

B. Enzymatic-based iron content measurement in liver extracts from both adult and aging animals with genotypes described in A.

C. Serum iron concentration measurement (same method as B) in animals described in B.

D. Transferrin saturation measurement in animals described in B.

E. Enzyme-linked immunosorbent assay (ELISA) of serum ferritin concentration in animals described in B.

(One way ANOVA test, *$p < 0.05$, **$p < 0.01$, ***$p < 0.001$. Each data point represents a single animal. Data presented as mean +SEM.)

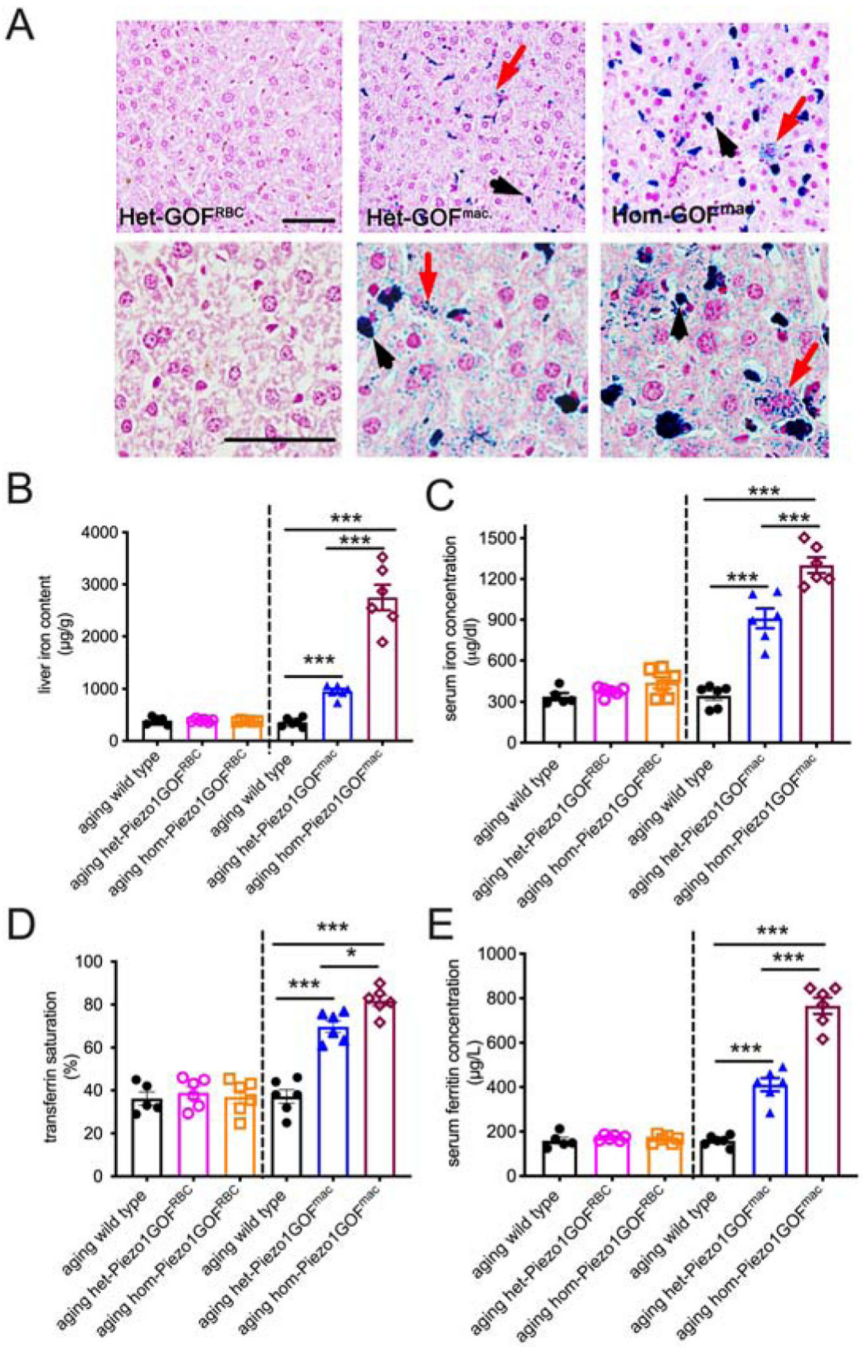

Figure 2.

GOF PIEZO1 expression in macrophages causes iron overload.

A. Perls Prussian blue staining in 10 μm paraffin sections of livers from aging RBC- and macrophage-specific GOF *Piezo1* mice (higher magnification examples shown in lower panels). Blue color represents iron in hepatocytes (red arrow) and Kupffer cells (black arrowhead). Note more iron staining in macrophage-specific GOF homozygotes compared to heterozygotes. (H&E staining used as background.Hom: homozygote; Het: heterozygote).

These mice were generated by breeding conditional GOF alleles to LysM-cre for targeting macrophages and EpoR-Cre for RBCs. Scale bars: 50 μm.

B. Enzymatic-based iron measurement in liver extracts from aging wild type and transgenic animals described in A.

C. Serum iron concentration measurement in animals described in B.

D. Transferrin saturation measurement in animals described in B.

E. Enzyme-linked immunosorbent assay (ELISA) of serum ferritin concentration in animals described in B.

(One way ANOVA test, *$p < 0.05$, **$p < 0.01$, ***$p < 0.001$. Each data point represents a single animal. Data presented as mean +SEM.)

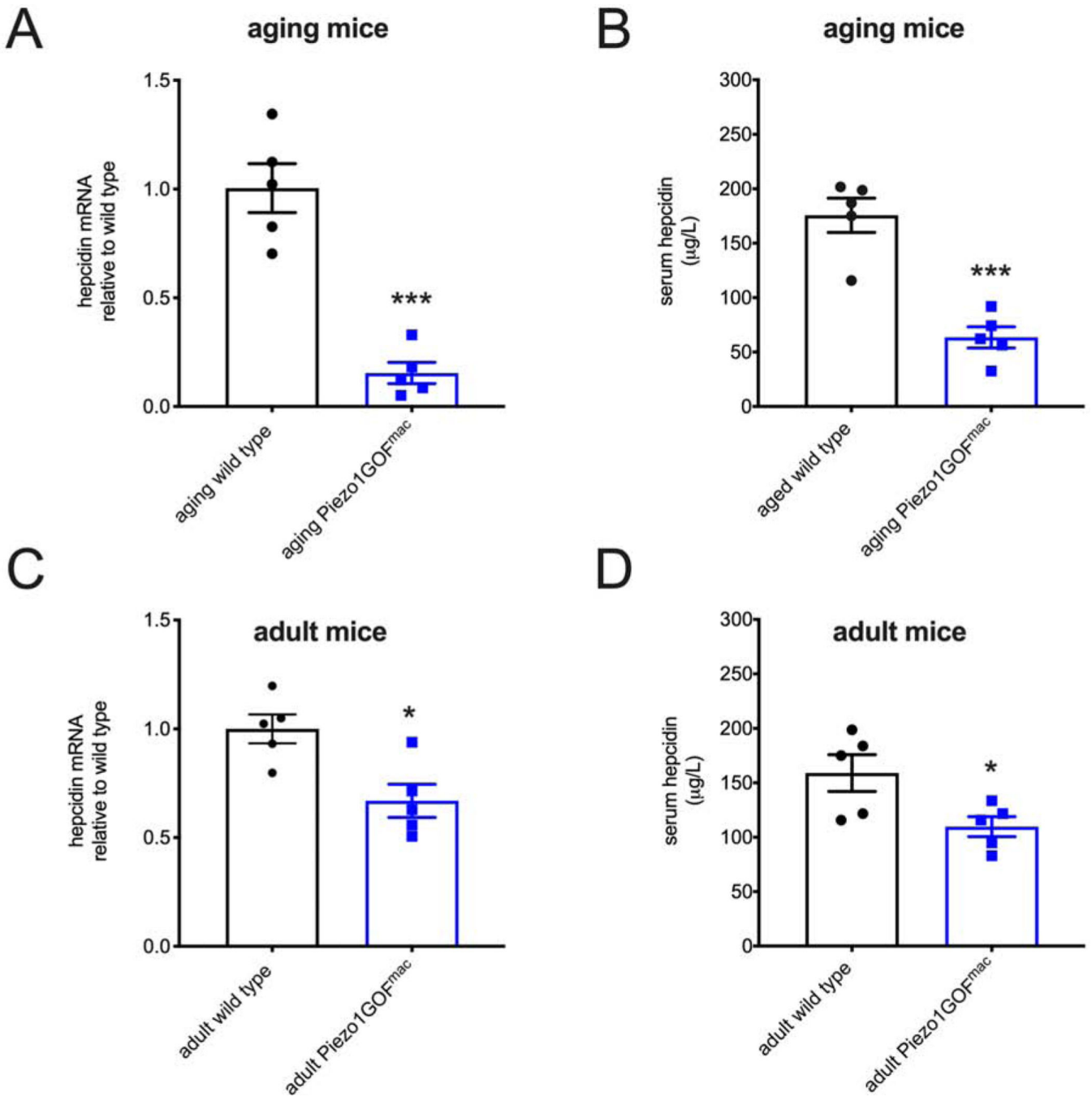

Figure 3.

Hepcidin levels are reduced in macrophage-specific GOF *Piezo1* mice.

A. Real-time RT-PCR analysis of liver expression of hepcidin mRNA from aging wild type and macrophage-specific GOF *Piezo1* mice (12 – 18 months old).

B. Enzyme-linked immunosorbent assay (ELISA) of serum hepcidin protein levels from animals described in A.

C. Real-time RT-PCR analysis of liver expression of hepcidin mRNA from adult wild type and macrophage-specific GOF *Piezo1* mice (2 – 5 months old).

D. ELISA of serum hepcidin protein levels from animals described in C.
(Student's t-tests, *p < 0.05, **p < 0.01, ***p < 0.001. Each data point represents a single animal. Data presented as mean +SEM)

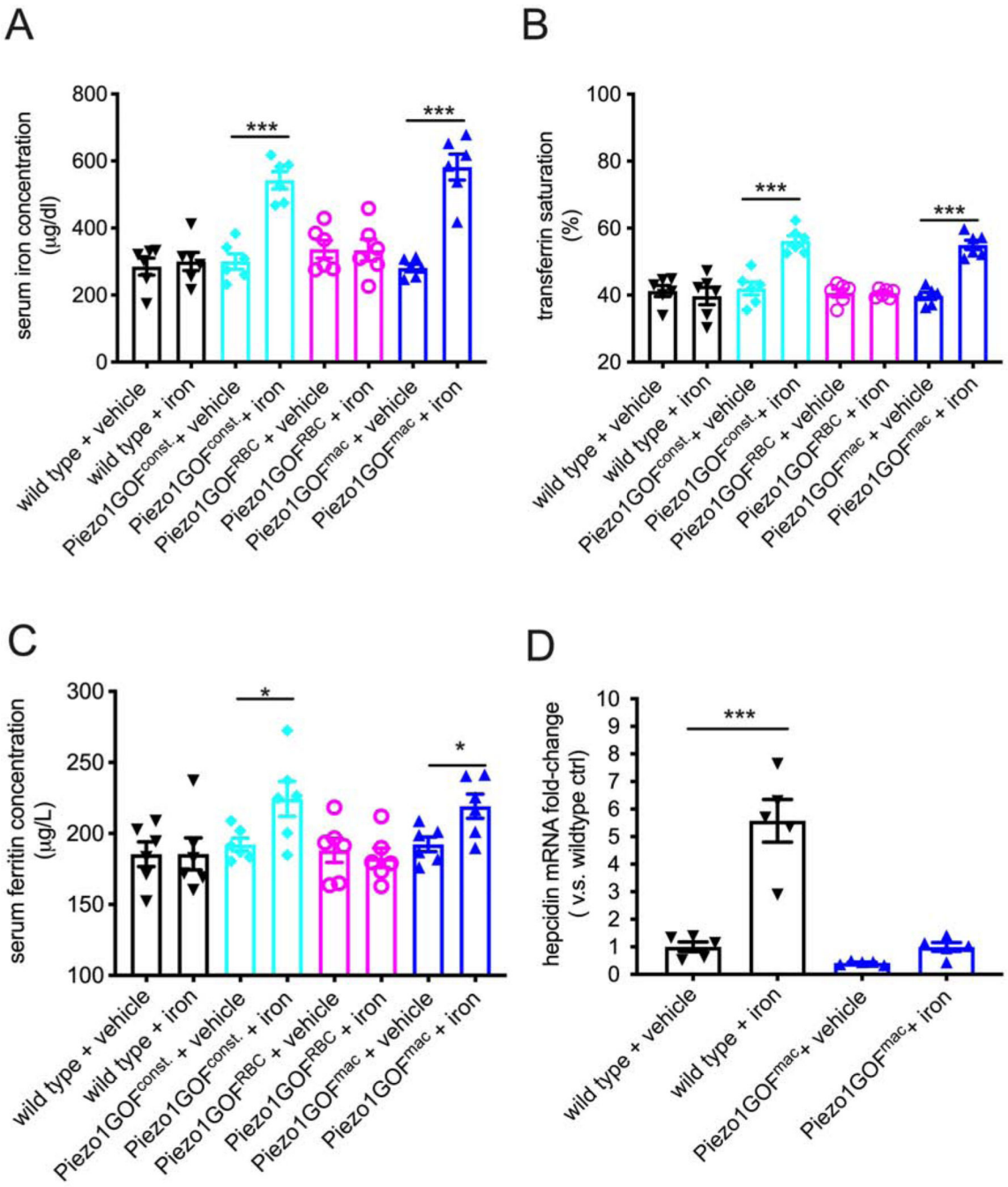

Figure 4.

Acute response to iron stress is compromised in macrophage-specific GOF *Piezo1* mice.

A. Serum iron levels in adult wild type, constitutive, RBC- and microphage-specific GOF *Piezo1* mice 24 hours after a single-dose injection of iron dextran at 40 μg/gram body weight.

B. Serum transferrin saturation as described in A.

C. Serum ferritin concentration as described in A.

D. Real-time RT-PCR analysis of liver expression of hepcidin mRNA as described in A.

(Dextran solution used as a vehicle control, multiple t-test with adjusted p-value by Bonferroni correction, *p < 0.05, **p < 0.01, ***p < 0.001. Each data point represents a single animal. Data presented as mean +SEM) (all RBC- and macrophage-specific GOF *Piezo1* mice are heterozygotes)

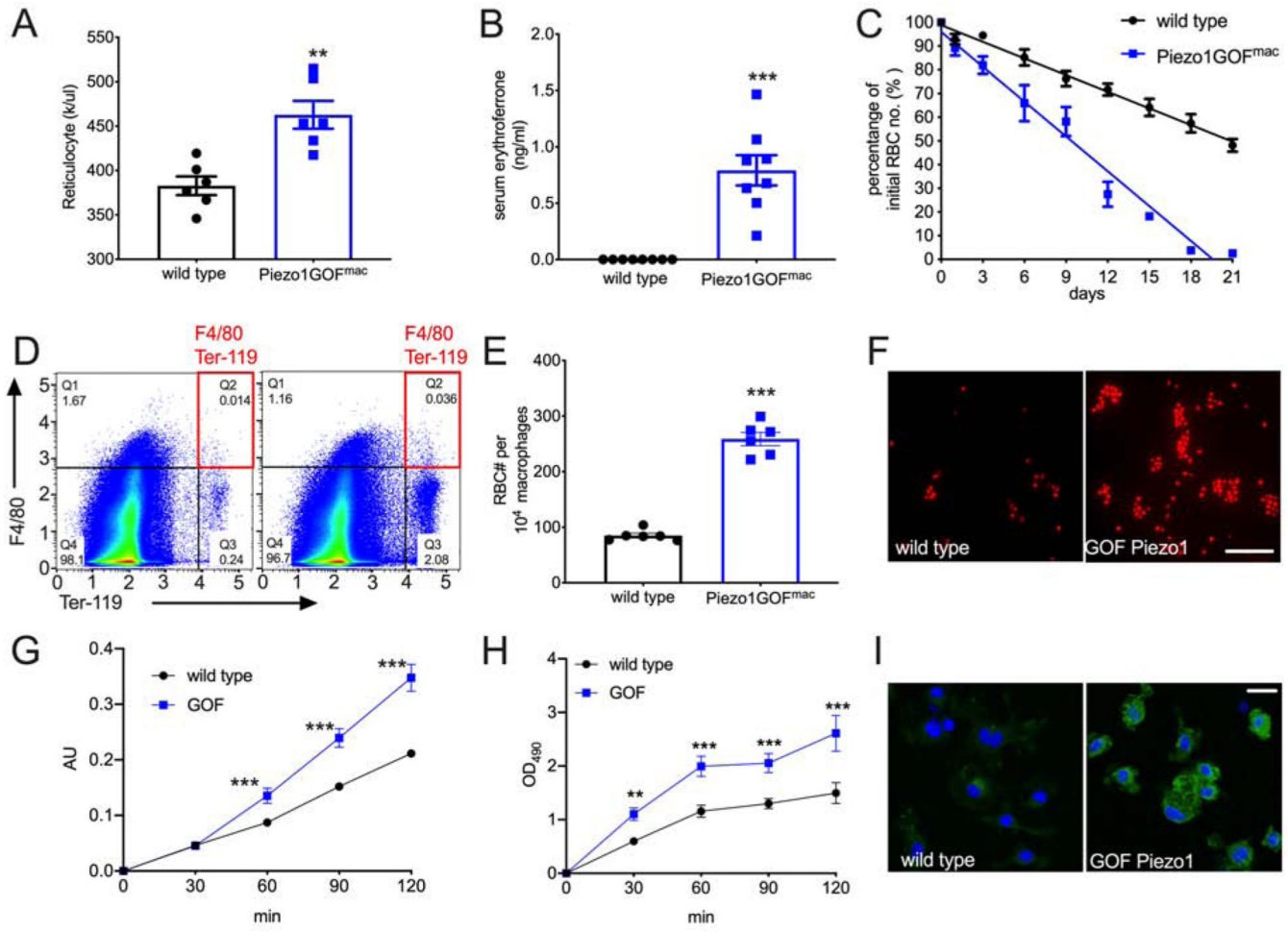

Figure 5.

Gain-of-function PIEZO1 in macrophages enhances erythropoiesis, red blood cell (RBC) turnover and phagocytic activity.

A. Reticulocyte count in whole blood. Unit: thousand per microliter

B. ELISA of serum erythroferrone concentration.

C. RBC turnover rate: pulse-chase experiment calculating percent fluorescent RBCs on a given day compared to number of fluorescent RBCs present initially on Day 1. The slope of linear best-fit curves represents RBC turnover rate.

D. Flow cytometry analysis for hemophagocytosis. F4/80 (y-axis) and Ter-119 (x-axis) label macrophages and RBCs respectively (axis values in log scale). Window Q2 have F4/80+; Ter-119+ cell populations which represent macrophages with internalized RBCs.

E. RBC numbers in splenic macrophages from D.

F. Fluorescent zymosan particles in wild type and GOF *Piezo1* macrophage culture.

G. Phagocytosis assay with opsonized RBCs. Arbitrary unit (AU) in absorption measures the amount of internalized RBCs in macrophages.

H. Rac1 activation assays during phagocytosis. OD values at 490nm represent active GTP-bound Rac1 levels in macrophage cell lysates.

I. Immunocytochemistry for active Rac1 in macrophages. Active Rac1 protein level is detected by specific antibody (green) in macrophage cytoplasm 30 min after phagocytosis. (Student t-tests, *p < 0.05, **p < 0.01, ***p < 0.001. Each data point represents a single animal in A-G, and represents a single cell in H and I. Data presented as mean +SEM, scale bar: 20μm)

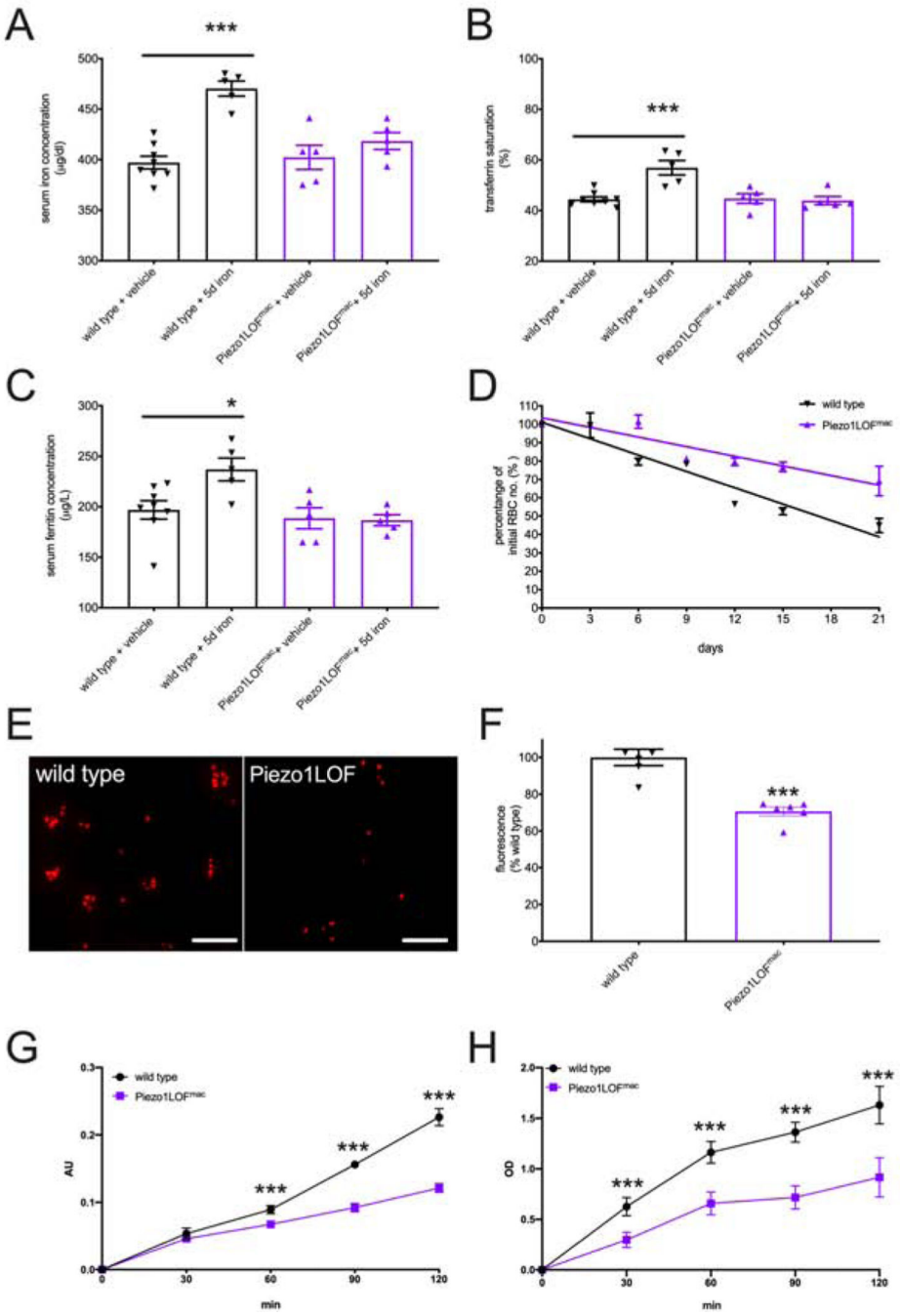

Figure 6.

PIEZO1 in macrophages is required for normal response to iron stress and phagocytosis.

A. Serum iron levels in adult wild type and macrophage-specific LOF *Piezo1* mice after daily injection of iron dextran at 80μg/gram body weight for 5 consecutive days.

B. Serum transferrin saturation as described in A.

C. Serum ferritin concentration as described in A.

D. RBC turnover rate *in vivo* measurement in 21 days for animals described in A (see Figure S4A).

E. *In vitro* phagocytosis assay: fluorescent zymosan particles in wild type and LOF *Piezo1* macrophage culture (See Figure S4B). Scale bar: 20μm.

F. Fluorescence intensity quantification of E (normalized to cell number).

G. Phagocytosis assay with opsonized RBCs and bone marrow derived macrophages. Arbitrary unit (AU) in absorption measures the amount of internalized RBCs in macrophages.

H. Rac1 activation assays during phagocytosis. OD values at 490nm represent active GTP-bound Rac1 levels in macrophage cell lysates.

(Dextran solution used as vehicle control, multiple t-test with adjusted p-value by Bonferroni correction, *$p < 0.05$, **$p < 0.01$, ***$p < 0.001$. Each data point represents a single animal in A-G, and represents a single cell in H. Data presented as mean +SEM)

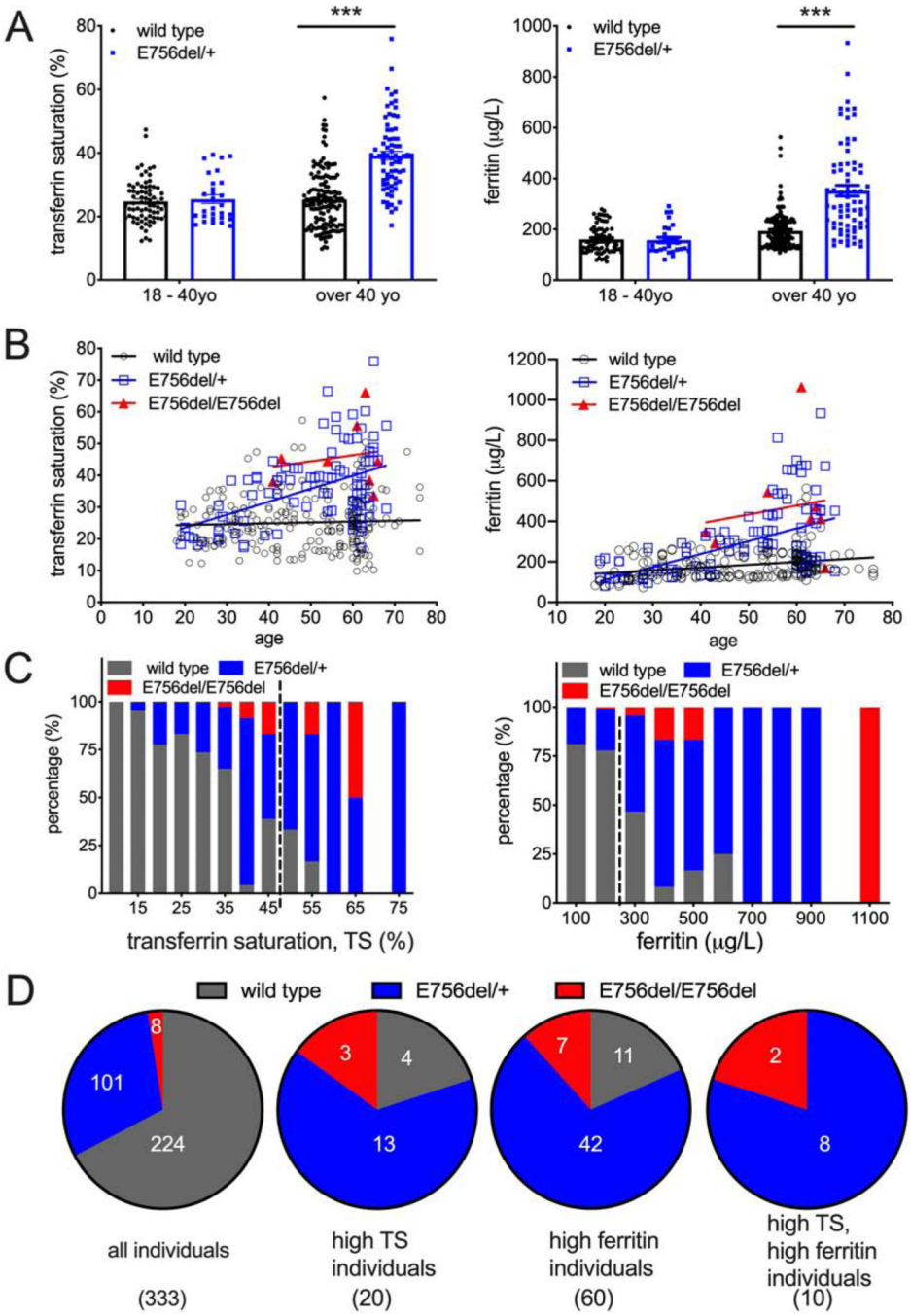

Figure 7.

E756del gain-of-function *PIEZO1* allele is associated with higher serum iron levels in an African American cohort.

A. Serum iron measurements in heterozygous *PIEZO1* E756del allele carriers and wild type of different age groups from a cohort of 333 African American individuals. Left: transferrin saturation. Right: ferritin.

B. Correlation between serum iron measurments and age in all three genotypes (wild type, E576del heterozygotes, and E576del homozygotes). Left: transferrin saturation. Right: ferritin.

C. Percentage of individuals in each serum iron measurement range for all three genotypes. Left: transferrin saturation. Right: ferritin. Values on the right of dashed line are clinically considered as provisionally high.

D. Frequency of genotypes in all individuals (left Pie chart) and individuals with provisionally high transferrin saturation (TS), ferritin, and both (Right three Pie charts). Actual number of individuals written in the chart.

(Student t-test, *$p < 0.05$, **$p < 0.01$, ***$p < 0.001$. Each data point represents a single human sample. Data presented as mean +SEM)

Key Resources Table

REAGENT or RESOURCE	SOURCE	IDENTIFIER
Antibodies		
AF647-conjugated F4/80	Biolegend	Catalog#123121
Alexa 488-conjugated CD68	Biolegend	Catalog#137011
PE-Dazzle 594-conjugated CD86	Biolegend	Catalog#105041
PE-conjugated CD163	Biolegend	Catalog#156703
BV711-conjugated MHC-II	Biolegend	Catalog#107643
BV421-conjugated TER119	Biolegend	Catalog#116233
eFluor450-conjugated CD3	Thermo Fisher	Catalog#48003742
eFluor450-conjugated CD19	Thermo Fisher	Catalog#48019382
eFluor450-conjugated NK1.1	Thermo Fisher	Catalog#48594182
Active Rac1-GTP	NewEast Biosciences	Catalog#26903
Bacterial and Virus Strains		
Mach1 competent cells	Thermo Fisher	Catalog#C862003
Biological Samples		
Healthy blood samples	Biological Specialty Corporation (Colmar, PA)	https://www.biospecialty.com/
Healthy blood samples	Lampire Biological Laboratories (Pipersville, PA)	http://www.lampire.com/
Chemicals, Peptides, and Recombinant Proteins		
Yoda1 (50mM stock) (Tocris)	Fisher Scientific	Catalog#5586/50
GsMTX4	Abcam	Catalog#141871
Critical Commercial Assays		
Total Iron-Bind Capacity (TIBC) kit	BioVision	K392–100
Mouse Ferritin ELISA kit	Abcam	ab157713
HEPCIDIN ELISA kit (mouse)	Aviva Systems Biology	OKEH01408
Mouse Erythroferrone ELISA Kit	Intrinsic LifeSciences	SKU:ERF-200
Rac1G-LISA Activation Assay Kit	Cytoskeleton Inc.	SKU: BK128
Mouse Inflammatory Cytokines Multi-Analyte ELISArray Kits	Qiagen	Catalog#336161
Human Hepcidin Quantikine ELISA kit	R&D Systems	DHP250
Human Ferritin ELISA kit	Sigma-Aldrich	RAB0197
CytoSelect 96-Well Phagocytosis Assay	Cell Biolabs	CBA-200

REAGENT or RESOURCE	SOURCE	IDENTIFIER
Experimental Models: Cell Lines		
Human Piezo1KO HEK cells	Our own lab	PMID: 28426961
Experimental Models: Organisms/Strains		
Mouse: B6.C-Tg(CMV-cre)1Cgn/J	The Jackson Laboratory	stock# 006054
Mouse: Epor$^{tm1(EGFP/cre)Uk}$	Dr. Klingmuller group at Max-Planck-Institute for Immunology, Freiburg, Germany	N/A
Mouse: B6.129P2-Lyz2$^{tm1(cre)Ifo}$/J	The Jackson Laboratory	stock# 004781
Mouse: GOF *Piezo1* conditional allele	Taconic Biosciences	Customized
Mouse: LOF Piezo1 conditional allele	The Jackson Laboratory	Stock#029213
Oligonucleotides		
GGCAAAGAGGCAAAATGTGC	This paper	RT-PCR forward primer for mhepcidin
TTGAGCTTGCTCTGGTGTCTGG	This paper	RT-PCR reverse for mhepcidin
CAGGCAGGATGCAGTGAGTG	This paper	Human E756del PCR
GGACATGGCACAGCAGACTG	This paper	Human E756del PCR
Recombinant DNA		
Plasmid: 3.2pc-IRES-tdTomato	This paper	N/A
Software and Algorithms		
Prism 8	GraphPad software	https://www.graphpad.com